The Approximate Fisher Influence Function: Faster Estimation of Data Influence in Statistical Models

Omri Lev and Ashia C. Wilson

MIT

Abstract

Quantifying the influence of infinitesimal changes in training data on model performance is crucial for understanding and improving machine learning models. In this work, we reformulate this problem as a weighted empirical risk minimization and enhance existing influence function-based methods by using information geometry to derive a new algorithm to estimate influence. Our formulation proves versatile across various applications, and we further demonstrate in simulations how it remains informative even in non-convex cases. Furthermore, we show that our method offers significant computational advantages over current Newton step-based methods.

1 Introduction

Understanding how a model's behavior changes with slight modifications to its training data is crucial for numerous machine-learning applications. These include detecting harmful patterns and constructing adversarial examples [27, 28, 6], conducting efficient cross-validation (CV) for model assessment and model selection [8, 51], enabling data unlearning without full retraining [44, 51], and evaluating robustness to data-dropping [10], among others. A common foundation for these tasks is the use of second-order approximations to capture the model's sensitivity to training data perturbations.

The most widely used technique in this space involves the Newton step, leveraging a gradient preconditioned by the inverse Hessian matrix. However, this approach can be computationally prohibitive and numerically unstable, particularly in high-dimensional and non-convex scenarios [30, 4]. As a computationally lighter alternative, several studies have explored influence approximations based on variants of the Fisher Information Matrix (FIM) [47, 41, 4, 23, 12]. Yet, despite growing empirical adoption, there remains a lack of theoretical understanding to guide the selection and use of FIM variants across diverse applications. Many of these works rely exclusively on the empirical FIM, which is known to underperform in several settings. Moreover, prior theoretical analyses of influence functions have largely assumed

Corresponding Author: omrilev@mit.edu

smooth, differentiable regularization—most commonly classical L_2—which limits their applicability in practical settings. Indeed, modern machine learning models frequently incorporate non-differentiable regularizers (e.g., ℓ_1 or group sparsity penalties), and recent work has shown that even certain neural networks can be framed as convex optimization problems with non-smooth regularization terms [39, 53]. This motivates the need for influence methods that are not only theoretically grounded but also scalable and valid under general, possibly non-smooth, regularizers—a gap that our work addresses.

In this paper, we propose the Approximate Fisher Influence Function (AFIF), a practical and theoretically justified framework for estimating influence in statistical models. AFIF leverages an approximation of the Fisher Information Matrix derived from exponential family structure, offering a computationally efficient alternative to Hessian-based methods. In contrast to prior influence techniques, which struggle with general regularization and lack formal guarantees for FIM-based approximations, our approach is provably accurate in convex settings and supports a broad range of regularization types—including non-differentiable ones.

Our main contributions are summarized as follows:

- **General Influence Estimation with Theoretical Guarantees:** We develop the Approximate Fisher Influence Function (AFIF), a theoretically grounded method for influence estimation that supports general regularization, including non-differentiable terms. Our analysis establishes the first theoretical guarantees for using FIM-based approximations in key influence tasks such as cross-validation and fairness evaluation—extending prior work limited to smooth, L_2-regularized settings.
- **Scalable FIM Approximation with Strong Empirical Performance:** We introduce a novel FIM variant derived from the exponential family structure that is both computationally efficient and theoretically justified. This formulation provides practical guidance on FIM selection. Empirically, AFIF matches the accuracy of Hessian-based methods while offering substantial improvements in speed and stability across diverse models and tasks.

Notation: Random variables are represented by sans-serif fonts $(\mathsf{x}, \mathsf{y}, \mathsf{z})$, and their realizations by regular italics (x, y, z). The PDF of z is $P_{\mathsf{z}}(\cdot)$. Sets of values are indicated by capital calligraphic letters, such as $\mathscr{D} \triangleq \{z_1, z_2, \dots, z_n\}$. Matrices are in bold capitals, with $\mathbf{I}_d$ as the $d \times d$ identity matrix. We use $f(x) = o(g(x))$ and $f(x) = O(g(x))$ when $f(x)/g(x) = 0$ and $f(x)/g(x) = c \neq 0$ in the limit $x \to \infty$. We denote the Lipschitz constant of a function f by $\text{Lip}(f) \triangleq \sup\{\|f(x) - f(y)\| / \|x - y\| : x \neq y \in \text{supp}(f)\}$. The inner product between two vectors θ_1 and θ_2 is denoted by $\theta_1^\top \theta_2 \triangleq \langle \theta_1, \theta_2 \rangle$.

2 Problem Statement

Given a dataset $\mathscr{D} = (z_1, z_2, \dots z_n)$ where each z_i is comprised of a covariate x_i and a label or response y_i, it is commonplace to use empirical risk minimization (ERM) to obtain a predictive model to deploy. In this work, we consider the problem of *weighted* ERM (wERM), i.e. given a loss function $\ell(\cdot)$, a regularizer $\pi(\cdot)$, a regularization parameter $\lambda \in [0, \infty)$ and a set of weights $w^n \triangleq (w_1, \ldots, w_n)$, our goal is to solve for $\hat{\theta}(w^n)$ that is defined as

$$\hat{\theta}(w^n) \triangleq \operatorname*{argmin}_{\theta} L(\mathscr{D}, \theta, \lambda, w^n), \tag{1}$$
$$L(\mathscr{D}, \theta, \lambda, w^n) \triangleq \frac{1}{n} \sum_{i=1}^{n} w_i \ell(z_i, \theta) + \lambda \pi(\theta).$$

This formulation is equivalent to classical ERM when $w^n = (1, \ldots, 1) \triangleq \mathbf{1}$, whose solution is denoted by $\hat{\theta}(\mathbf{1})$ [1].

In many scenarios $\ell(z, \theta) = -\log(P(y|f(x; \theta)))$; that is, the loss can be interpreted as a negative log-likelihood under a probabilistic model induced by a parameterized function $f(x; \theta)$, often taken to be a neural network. Moreover, we study the case where $P(y|f(x; \theta))$ belongs to an *exponential-family* [50] whose natural parameters are $f(x; \theta)$ and whose natural statistics are denoted by $t(y)$, namely, $\log(P(y|f(x; \theta))) = f(x; \theta)^\top t(y) - \log(\sum_{\tilde{y} \in \mathcal{Y}} \exp(f(x; \theta)^\top t(\tilde{y}))) + \beta(y)$ for some function $\beta(y)$. This is satisfied by many common loss functions in machine learning (see popular examples for such losses in App. B).

Remark 1. Following [5], this class of losses corresponds to loss functions that can be captured by a Bregman divergence up to an additional term that is independent of $f(x; \theta)$. See further discussion in App. B.

2.1 Inference Objective

We study the *inference objective*, $T(\cdot, \cdot) : \mathbb{R}^d \times \mathbb{R}^n \to \mathbb{R}^k$, which maps a parameter vector θ and a weight vector w^n to a desired inference target, where w^n belongs to a family of weight vectors $\mathcal{W}$. In particular, we focus on cases where w^n corresponds to a leave-one-out weight vector, defined as

$$\mathscr{D}^{-i} \triangleq \{w^n : w_j = \mathbb{1}\{j \neq i\}\}.$$

This formulation captures a range of tasks, including:

Cross Validation To assess and select models, leave-one-out cross-validation (LOOCV) estimates model performance by iterative training on all but one data point and evaluating on the omitted instance. Specifically, for each i, it computes the evaluation metric:

$$T(\hat{\theta}(w^n), w^n) \triangleq \frac{1}{n} \ell(z_i, \hat{\theta}(w^n)) \quad \text{for} \quad w^n \in \mathscr{D}^{-i},$$

where $\mathscr{D}^{-i}$ denotes the leave-one-out weight vectors, $\hat{\theta}(w^n)$ is the model trained with w^n, and the corresponding evaluation is taken on the omitted sample. Leave-k-out cross-validation follows analogously by removing a subset of k observations in each iteration [19, 48].

[1] Throughout, we simplify our notation by omitting the explicit dependence on λ when possible. For example, we write $L(\mathscr{D}, \theta, w^n)$ instead of $L(\mathscr{D}, \theta, \lambda, w^n)$ whenever $\lambda = 0$.

Machine Unlearning To remove the influence of a data point z_i, the “unlearned model” is obtained by computing

$$T(\hat{\theta}(w^n), w^n) = \hat{\theta}(w^n) \quad \text{for} \quad w^n \in \mathscr{D}^{-i}.$$

This ensures that the model parameters are updated as if z_i were never included in training [11, 52]. Similarly, unlearning k data points follows the same formulation using leave-k-out weight vectors.

Data attribution Understanding the contribution of a training sample $z_i \in \mathscr{D}$ to a model's prediction on a test point z_{test} [27] is formulated as comparing $\ell(z_{\text{test}}, \hat{\theta}(\mathbf{1}))$ with

$$T(\hat{\theta}(w^n), w^n) = \ell(z_{\text{test}}, \hat{\theta}(w^n)) \triangleq T(\hat{\theta}(w^n)) \quad \text{for} \quad w^n \in \mathscr{D}^{-i}.$$

Attribution to a set of k points follows analogously.

Fairness Evaluation Ghosh et al. [20] propose to evaluate the impact of z_i on model fairness by computing $T(\hat{\theta}(w^n))$ for $w^n \in \mathscr{D}^{-i}$, where T is a chosen fairness metric. For example, if we have a dataset $\{x_i\}_{i=1}^n$ with binary sensitive attributes $\{s_i\}_{i=1}^n$, robustness with respect to *demographic parity*—which assesses whether the model's predictions are independent of a sensitive attribute s—is given by:

$$\begin{aligned} &T(\hat{\theta}(w^n), w^n) \triangleq T(\hat{\theta}(w^n)) \\ &\quad T(\hat{\theta}(w^n)) = |\mathbb{E}_{\hat{P}(\mathsf{x}|\mathsf{s}=0)}[f(\mathsf{x}; \hat{\theta}(w^n))] - \mathbb{E}_{\hat{P}(\mathsf{x}|\mathsf{s}=1)}[f(\mathsf{x}; \hat{\theta}(w^n))]|, \quad \text{for } w^n \in \mathscr{D}^{-i}. \end{aligned} \tag{2}$$

Here, $\hat{P}(\mathsf{x} = x|\mathsf{s} = s)$ is the empirical distribution for $s \in \{0, 1\}$. For cases where the sensitive attributes $\{s_i\}$ are continuous-valued, an alternative fairness metric can be defined via the χ^2 divergence [36, 46]. A popular choice for such a metric is defined via

$$\begin{aligned} &T(\hat{\theta}(w^n), w^n) \triangleq T(\hat{\theta}(w^n)) \\ &\quad T(\hat{\theta}(w^n)) = \chi^2 \left(\widehat{P}_{f(\mathsf{x};\hat{\theta}(w^n)),\mathsf{s}} \| \widehat{P}_{f(\mathsf{x};\hat{\theta}(w^n))} \widehat{P}_{\mathsf{s}} \right), \quad \text{for } w^n \in \mathscr{D}^{-i}. \end{aligned} \tag{3}$$

The impact of removing a subset of k samples is assessed analogously by considering $w^n \in \mathscr{D}^{-K}$.

2.1.1 Inference Approximation

Since $\hat{\theta}(w^n)$ for each weight vector is often computationally expensive, many methods approximate the inference objective using quantities derived from $\hat{\theta}(\mathbf{1})$. That is, instead of solving for $\hat{\theta}(w^n)$ directly, we use an approximation that combines the known vector $\hat{\theta}(\mathbf{1})$ with a function of the weights w^n:

$$\hat{\theta}(w^n) \approx g(\hat{\theta}(\mathbf{1}), w^n) \triangleq \tilde{\theta}(w^n).$$

Typically, $g(\cdot, \cdot)$ is derived from a Taylor series expansion around $\hat{\theta}(\mathbf{1})$, capturing the pth-order sensitivity of the model parameters to small perturbations in w^n. Depending on p, this allows for efficient approximation without requiring full retraining [22, 21, 51]. Two widely used approaches to approximate the inference objective $T(\hat{\theta}(w^n), w^n)$ are:

1. **Plug-in Estimator**: This approach directly substitutes the approximation $\tilde{\theta}(w^n)$ into the inference objective:

$$T(\hat{\theta}(w^n), w^n) \approx T(\tilde{\theta}(w^n), w^n) = T(g(\hat{\theta}(\mathbf{1}), w^n), w^n).$$

2. **Linearized Influence Approximation**: Instead of replacing $\hat{\theta}(w^n)$ directly, this method uses a first-order expansion of $T(\hat{\theta}(w^n), w^n)$ around $\hat{\theta}(\mathbf{1})$. The approximation function $g(\cdot,\cdot)$ is then incorporated into this expansion to estimate $\hat{\theta}(w^n)$:

$$T(\hat{\theta}(w^n), w^n) \approx T(\hat{\theta}(\mathbf{1}), w^n) + \langle \nabla_\theta T(\hat{\theta}(\mathbf{1}), w^n), \tilde{\theta}(w^n) - \hat{\theta}(\mathbf{1}) \rangle. \tag{4}$$

Both methods are shown in several works to reduce computational overhead while maintaining strong empirical performance [27, 28, 51, 6]. However, the quality of the approximation depends on how well $g(\cdot,\cdot)$ captures the true parameter updates. In the next section, we introduce a new method for creating such an approximation.

3 The Approximate Fisher Influence Function

In this section, we introduce our proposed method and describe how it improves the computational efficiency of the currently existing baselines.

A common approach to approximating $\hat{\theta}(w^n)$ is to optimize a surrogate to the loss function $L(\mathscr{D}, \theta, \lambda, w^n)$. This paper focuses on methods based on *quadratic approximations of the objective* [13, 27, 22, 51], which provide computationally efficient estimates while maintaining accuracy. These approximations yield solutions of the form:

$$\tilde{\theta}(w^n) = \hat{\theta}(\mathbf{1}) - \mathbf{C}(\hat{\theta}(\mathbf{1}), w^n) b(\hat{\theta}(\mathbf{1}), w^n),$$

where $b(\cdot,\cdot)$ and $\mathbf{C}(\cdot,\cdot)$ depend on the specific loss approximation and vary across applications.

A notable instance of this framework is the *infinitesimal jackknife* (IJ) approximation [22], denoted $\tilde{\theta}^{\mathrm{IJ}}(w^n)$, which is defined via a Newton step:

$$\begin{aligned} b(\hat{\theta}(\mathbf{1}), w^n) &\triangleq \frac{1}{n}\sum_{i=1}^{n} \nabla_\theta \ell(z_i, \hat{\theta}(\mathbf{1}))(w_i - 1), \\ \mathbf{C}(\hat{\theta}(\mathbf{1}), \mathbf{1}) &= \nabla_\theta^2 L(\mathscr{D}, \hat{\theta}(\mathbf{1}), \mathbf{1})^{-1} \triangleq \mathbf{H}(\hat{\theta}(\mathbf{1}), \mathbf{1})^{-1}. \end{aligned} \tag{5}$$

In this work, we suggest a modified computationally efficient second-order approximation of $\hat{\theta}(w^n)$ using the *natural gradient*. We consider loss functions ℓ that represent the log-likelihood of a parametric probabilistic model, $\ell(z,\theta) = -\log(P_{\mathsf{y}|\mathsf{x}}(y|f(x;\theta)))$, where $P_{\mathsf{y}|\mathsf{x}}(y|f(x;\theta))$ lies on the probability simplex of the output alphabet $\mathcal{Y}$ and is parameterized by θ [3, 2, 5]. As discussed by [5] (see also App. B), this property holds for a large class of losses in machine learning. While the standard gradient identifies the direction that minimizes the objective based on Euclidean distance, the natural gradient accounts for the underlying geometry (curvature) of the parameter space. This is achieved by pre-multiplying the gradient with the inverse of the FIM, which characterizes the sensitivity of the model's likelihood function to changes in parameters. To that end, the Hessian in (5) is replaced by:

$$g_{\mathsf{y}|\mathsf{x}} \triangleq \nabla_\theta \log(P_{\mathsf{y}|\mathsf{x};\theta}(\mathsf{y}|\mathsf{x}; \hat{\theta}(\mathbf{1}))),$$
$$\mathbf{F}(\hat{\theta}(\mathbf{1})) \triangleq \mathbb{E}_{(\mathsf{x},\mathsf{y})\sim P_{\mathsf{x},\mathsf{y};\theta=\hat{\theta}(\mathbf{1})}}[g_{\mathsf{y}|\mathsf{x}} \cdot g_{\mathsf{y}|\mathsf{x}}^\top],$$

where $P_{\mathsf{y}|\mathsf{x}}$ is the probabilistic model induced by the loss function [35]. However, since the covariate distribution P_{x} is typically unknown, direct computation of the expectation is infeasible. Instead, we approximate the FIM using empirical estimates, averaging over the observed covariates and leveraging the network structure to evaluate expectations over $P_{\mathsf{y}|\mathsf{x};\theta}$ [35, 30]. The resulting *approximate FIM* is given by:

$$\mathbf{F}(\mathscr{D}, \hat{\theta}(\mathbf{1})) \triangleq \frac{1}{n} \sum_{x \in \mathscr{D}} \mathbb{E}_{\mathsf{y}\sim P_{\mathsf{y}|\mathsf{x}=x;\theta=\hat{\theta}(\mathbf{1})}}[g_{\mathsf{y}|\mathsf{x}} \cdot g_{\mathsf{y}|\mathsf{x}}^\top].$$

Using this approximation, we define the *Approximate Fisher Infinitesimal Jackknife* similarly to (5), replacing $\mathbf{C}$ with the approximate FIM $\mathbf{F}(\mathscr{D}, \hat{\theta}(\mathbf{1}))$:

$$\tilde{\theta}^{\mathrm{IJ,AF}}(w^n) \triangleq \hat{\theta}(\mathbf{1}) - (\mathbf{F}(\mathscr{D}, \hat{\theta}(\mathbf{1})))^{-1} b(\hat{\theta}(\mathbf{1}), w^n). \tag{6}$$

Following classical results [43, 35], when the loss function is given by $\ell(z, \theta) = -\log(P\,(y|f(x;\theta)))$ and $P(y|f)$ belongs to an exponential family, the approximate FIM can be interpreted as a positive semi-definite (PSD) approximation of the Hessian. Specifically, the Hessian satisfies:

$$\mathbf{H}(\hat{\theta}(\mathbf{1}), \mathbf{1}) = \mathbf{F}(\mathscr{D}, \hat{\theta}(\mathbf{1})) + \mathbf{R},$$

where $\mathbf{F}(\mathscr{D}, \hat{\theta}(\mathbf{1}))$ is guaranteed to be PSD, and the remainder term is given by:

$$\frac{1}{n} \sum_{i=1}^{n} \nabla_\theta^2 f(x_i; \hat{\theta}(\mathbf{1})) \nabla_f \log(P(y_i|f(x_i; \hat{\theta}(\mathbf{1})))).$$

This remainder term can be non-zero, for example, in cases where $f(x;\theta)$ is non-linear in θ. However, in many settings, including commonly used models, $\mathbf{R}$ shrinks to zero (in L_2 sense) as training accuracy improves [30, 35] (see App. B, App. E). Thus, the approximated FIM is often viewed as a computationally efficient PSD approximation of the Hessian.

3.1 Computational Savings

Here, we show a fundamental efficiency improvement in evaluating (6) compared to the IJ approach (5). Both methods require computing expressions of the form $\mathbf{A}^{-1} b(\hat{\theta}(\mathbf{1}), w^n)$ where $\mathbf{A} = \mathbf{F}(\mathscr{D}, \hat{\theta}(\mathbf{1}))$ in (9) and $\mathbf{A} = \mathbf{H}(\hat{\theta}(\mathbf{1}), \mathbf{1})$ for the IJ. Since directly inverting a large $d \times d$ matrix is infeasible, efficient computation of inverse-matrix-vector products is essential. However, since the FIM requires only first-order differentiation through the model, it will typically be much more computationally efficient relative to the Hessian-based alternative. To that end, we will now demonstrate a fundamental computational efficiency of using the FIM over the Hessian in a widely used influence calculation setting invented by the classical work of [27] and involves stochastic estimation of inverse-matrix-vector products via the `LiSSA` algorithm [1]. Similar computational benefits are further applied in modern existing variants of influence measurement techniques that rely on variants of the `LiSSA` algorithm, and stochastic estimation of inverse matrix-vector products, such as [24, 42].

3.1.1 Stochastic Estimation

Stochastic estimation techniques rely on generating a sequence of estimators $v_j \triangleq (\widehat{\mathbf{A}^{-1}x})_j$ that converge in expectation to $\mathbf{A}^{-1}x$ as $j \to \infty$, where each v_j utilizes only a small batch of training data, yielding a computationally tractable way to estimate $\mathbf{A}^{-1}x$. As an example of the computational superiority of the FIM-based methods, we will demonstrate the improvement for the celebrated `LiSSA` algorithm [1] that approximates $\mathbf{A}^{-1}$ using the truncated Neumann series $\mathbf{A}_j^{-1} = \sum_{i=0}^{j}(\mathbf{I} - \sigma\mathbf{A})^i$ for some $\sigma > 0$ [2]. This approximation is computed via the recursion $\mathbf{A}_j^{-1} = \mathbf{I} + (\mathbf{I} - \sigma\mathbf{A})\mathbf{A}_{j-1}^{-1}$. Consequently, each v_j is defined by $v_j = x + (\mathbf{I} - \sigma\mathbf{A})v_{j-1}$ with $v_0 = x$ and final estimate $v = \sigma v_N$. The major computational hurdle is multiplying by $\mathbf{A}$. When $\mathbf{A}$ depends on many training points (e.g., $\mathbf{F}(\mathscr{D}, \hat{\theta}(\mathbf{1}))$ or $\mathbf{H}(\hat{\theta}(\mathbf{1}), \mathbf{1})$), it is typical to estimate it by using a sampled batch of training data. We now analyze the computational complexity of these calculations for each method.

Estimation with $\mathbf{F}(\mathscr{D}, \hat{\theta}(\mathbf{1}))$. When $\mathbf{A} \triangleq \mathbf{F}(\mathscr{D}, \theta)$, each $\mathbf{A}v_j$ requires calculating

$$\nabla_\theta f_i \cdot (\nabla_f^2 \log(P(y_i|f_i)))(v_j^\top \nabla_\theta f_i)^\top) \tag{7}$$

where $f_i \triangleq f(x_i; \theta)$. Given the form of $\nabla_f^2 \log(P(y_j|f(x_j;\theta)))$ (see App. B), computing this expression requires the vector-Jacobian product (VJP) $a_j = v_j^\top \nabla_\theta f_i$ and the Jacobian-vector product (JVP) $\nabla_\theta f_i \cdot (\nabla_f^2 \log(P(y_i|f_i)))a_j^\top)$.

Estimation with $\mathbf{H}(\hat{\theta}(\mathbf{1}), \mathbf{1})$. For $\mathbf{A} \triangleq \mathbf{H}(\hat{\theta}(\mathbf{1}), \mathbf{1})$, each $\mathbf{A}v_j$ requires computing,

$$\nabla_\theta^2 \log(P(y_i|f_i))v_j, \tag{8}$$

which requires computing a Hessian-vector product (HVP) with respect to all model parameters.

Comparing Computations. Computing (8) requires roughly four evaluations of the entire model [43, 14]. In contrast, a JVP can be computed in a single forward pass using forward-mode automatic differentiation [9]. Since $\nabla_f^2 \log(P(y_i|f_i))$ is typically simple and depends only on the number of model outputs (not on d), evaluating (7) requires just one differentiation in backward mode. Furthermore, given backward differentiation roughly requires twice the complexity of model evaluation [16, 14], this method significantly reduces FLOPs and accelerates computations. We demonstrate these savings through simulations in Sec. 5. We summarize the results in Tbl. 1.

Remark 2. Although our analysis focuses on the `LiSSA` algorithm, the fact that the FIM depends solely on first-order gradients means these improvements are broadly applicable to many methods that require differentiating through a large model using the structure of the curvature matrix. For example, similar fundamental gains were observed in [41] by employing efficient matrix-inversion techniques based on rank-one updates.

[2] σ is usually a small positive constant to stabilize calculations.

	Forward	Backward	FLOPs
(8)	0	2	$O(4F)$
(8)	2	1	$O(4F)$
(7)	1	1	$O(3F)$

Table 1: Number of differentiations in forward mode, backward mode, and FLOPs required to evaluate (7) and (8), for different evaluation options from [14]. F denotes the FLOPs needed for a single model evaluation.

4 Theoretical Analysis

This section presents a general theoretical framework for analyzing the accuracy of inference objective approximations based on plug-in estimates and linearization approximations and based on the FIM. Specifically, we establish conditions under which these approximations remain close, in a well-defined sense, to the true inference function when the loss function satisfies certain regularity properties. While similar results are well understood for infinitesimal jackknife-based approximations, our framework extends these findings to also cover settings when one replaces the Hessian with the approximated FIM.

4.1 Related work

Several works have established the accuracy of this approximation under specific conditions on the loss function and the weight vectors w^n [22, 51, 49, 44]. These results hold under subsets of the following assumptions.

Assumption 1 (Curvature of the Objective). For each $i \in [n]$, the function $\frac{1}{n}\ell(z_i, \theta)$ is μ-strongly convex ($\mu > 0$), and the prior $\pi(\theta)$ is convex.

Assumption 2 (Lipschitz Hessian of the Objective). For each $i \in [n]$, the function $\frac{1}{n}\ell(z_i, \theta)$ is twice differentiable with an M-Lipschitz Hessian.

Assumption 3 (Smooth Hessian of the Objective). For each $i \in [n]$, the function $\frac{1}{n}\ell(z_i, \theta)$ is twice differentiable with a C-smooth Hessian.

Assumption 4 (Bounded Moments). For given $s, r \geq 0$, the quantity B_{sr} is finite, where

$$B_{sr} \triangleq \frac{1}{n}\sum_{i=1}^{n} \mathrm{Lip}(\nabla_\theta \ell(z_i, \cdot))^s \|\nabla_\theta \ell(z_i, \hat{\theta}(\mathbf{1}))\|^r.$$

Assumption 5 (Lipschitz Features). The feature mapping $f(x_i; \theta)$ is C_f-Lipschitz with a $\tilde{C}_f$-Lipschitz gradient for all $i \in [n]$.

Assumption 6 (Lipschitz Inference Objective). The inference objective $T(\theta, w^n)$ is twice differentiable, C_{T_1}-Lipschitz, and has a C_{T_2}-Lipschitz gradient with respect to θ for $w^n \in \mathscr{D}^{-i}$ and all $i \in [n]$.

For the examples in Sec. 2, the following guarantees were proved to hold under subsets of Assump. 1-Assump. 6:

Proposition 1 (LOOCV Approximation Bound ([51], Thm. 4))**.** *Suppose Assump. 1, Assump. 2, and Assump. 4 hold for* $(s, r) = \{(0, 3), (1, 3), (1, 4), (1, 2), (2, 2), (3, 2)\}$*. When the IJ is used as a plug-in estimate for the LOOCV objective*

$$T_i(\theta) \triangleq T(\theta, w^n) = \frac{1}{n}\ell(z_i, \theta),$$

with $w^n \in \mathscr{D}^{-i}$*, the error in this approximation is bounded as*

$$\left| \sum_{i=1}^{n} \left(T_i(\tilde{\theta}^{\mathrm{IJ}}(w^n)) - T_i(\hat{\theta}(w^n)) \right) \right| = O\left(\frac{MB_{03}}{\mu^3 n^2} + \frac{B_{12}}{\mu^2 n^2} \right).$$

The next proposition relies on the (ε, δ)-unlearning definition from [44].

Proposition 2 (Machine Unlearning [49])**.** *Suppose* $\ell(z, \theta)$ *is* μ*-strongly convex, twice differentiable,* L*-Lipschitz, with a* C*-smooth and* M*-Lipschitz Hessian for all* z*, and that* $\pi(\theta)$ *is convex.*[3] *When the IJ is used as a plug-in estimate for the objective* $T(\theta) = \theta$*, we have*

$$\|T(\tilde{\theta}^{\mathrm{IJ}}(w^n)) - T(\hat{\theta}(w^n))\| \leq \frac{2ML}{n^2\mu^2} + \frac{CL^2}{n^2\mu^3}, \quad \textit{for } w^n \in \mathscr{D}^{-i}.$$

Furthermore, the algorithm returning $\tilde{\theta}^{\mathrm{IJ}}(w^n) + \zeta$ *for* $w^n \in \mathscr{D}^{-i}$ *satisfies* (ε, δ)*-unlearning, where* $\zeta \sim \mathcal{N}(0, c\mathbf{I})$ *with* $c = (2\mu ML + CL^2)\sqrt{2\log(5/4\delta)}/\varepsilon\mu^3 n^2$.

Proposition 3 (Data Attribution ([28], Prop. 1))**.** *Suppose Assump. 1, Assump. 2, and Assump. 6 hold, and that* $\pi(\theta) = \|\theta\|^2$*. Define* $C_\ell \triangleq \max_{i\in[n]} \|\nabla \ell(z_i, \hat{\theta}(\mathbf{1}))\|$*. When the IJ is used as a plug-in estimate for the inference objective*

$$T(\theta) = \ell(z_{\text{test}}, \theta) - \ell(z_{\text{test}}, \hat{\theta}(\mathbf{1})),$$

the approximation error is bounded as

$$\left| T(\hat{\theta}(w^n)) - T(\tilde{\theta}^{\mathrm{IJ}}(w^n)) \right| \leq \frac{MC_{T_1}C_\ell^2}{n^2\mu^3}, \quad \textit{for } w^n \in \mathscr{D}^{-i}.$$

While certain loss functions may not be Lipschitz, Assump. 2 and Assump. 4 require only that the *normalized* losses evaluated on the training set satisfy Lipschitz continuity— a condition that generally holds in practice [22, Assump. 3]. Similarly, when the inference objective is of the form $\ell(z_{\text{test}}, \theta)$, Lipschitz continuity is required only with respect to the test point z_{test}. As long as z_{test} is not pathological, this assumption is typically satisfied.[4]

Additionally, the framework in [22] assumes differentiable regularization. In certain cases, similar approximations extend to settings where the regularizer is non-differentiable [51, 49].

[3] These assumptions strengthen Assump. 1-Assump. 4, requiring Lipschitz continuity for any z, not just the training samples $\{z_i\}$.

[4] The assumption that T is Lipschitz is consistent with classical works on influence functions; see [28, Prop. 1].

4.2 The Approximate Fisher Influence Function

We now present the *approximate Fisher influence* and its theoretical characterization. First, we introduce an additional technical assumption about the loss function, which is essential for our proofs.

Assumption 7. The loss functions are of the form $\ell(z,\theta) = -\log(P(y|f(x;\theta)))$ where $P(y|f)$ belongs to a regular exponential family whose natural parameters are $f(x;\theta)$. Moreover, we further assume that $\left\|\nabla_f^2 \log\left(P\left(y|f(x;\theta)\right)\right)\right\| \leq Q$ for some $Q > 0$.

To accommodate non-smooth regularizers, we utilize the *proximal operator*, defined as:

$$\operatorname{prox}_{\lambda\pi}^{\mathbf{D}}(v) \triangleq \underset{\theta}{\operatorname{argmin}} \left\{(v-\theta)^\top \mathbf{D}(v-\theta) + 2\lambda\pi(\theta)\right\}.$$

Our main lemma, Lem. 1, defines the approximate Fisher influence and bounds its discrepancy from $\hat{\theta}(w^n)$ for $w^n \in \mathscr{D}^{-i}$.

Lemma 1. *Suppose Assump. 1, Assump. 2, Assump. 5, and Assump. 7 hold. Define* $\bar{E}_n \triangleq \sum_{j=1}^n \|\nabla_f \log(P(y_j|f(x_j;\hat{\theta}(\mathbf{1}))))\|$, $\tilde{g}_i \triangleq \|\nabla_\theta \ell(z_i,\hat{\theta}(\mathbf{1}))\|$ *and* $g_i = \tilde{g}_i/n$. *Then, the approximated Fisher influence function, defined via*

$$\tilde{\theta}(w^n) = \operatorname{Prox}_{\lambda\pi}^{\mathbf{F}(\mathscr{D},\hat{\theta}(\mathbf{1}))}(\tilde{\theta}^{\mathrm{IJ,AF}}(w^n)), \quad \text{for } w^n \in \mathscr{D}^{-i}. \tag{9}$$

satisfies

$$\|\tilde{\theta}(w^n) - \hat{\theta}(w^n)\| \leq \frac{2QC_f^2\tilde{g}_i}{n^2\mu^2} + \frac{M\tilde{g}_i^2}{n^2\mu^3} + \frac{2\tilde{g}_i\tilde{C}_f\bar{E}_n}{n\mu^2}, \quad \text{for } w^n \in \mathscr{D}^{-i}. \tag{10}$$

Proof sketch. The proof separately bounds the distances between (i) $\hat{\theta}(w^n)$ and $\tilde{\theta}^{\mathrm{IJ}}(w^n)$, and (ii) $\tilde{\theta}^{\mathrm{IJ}}(w^n)$ and $\tilde{\theta}^{\mathrm{IJ,AF}}(w^n)$ for $w^n \in \mathscr{D}^{-i}$. The first bound follows from [51, Lem. 1], while the second leverages the closeness of the Hessian and the FIM to show that the estimates remain close. Full proof is provided in App. E. □

Similar to prior results [51, 49, 44], the first two terms in (10) depend on global problem constants (Lipschitz coefficients, strong convexity parameter, etc.) and the gradient at the ith training point. The third term depends on $\bar{E}_n$, which simplifies due to the exponential family structure of the loss and is given by (see App. G)

$$\|\nabla_f \log(P(y_i|f(x_i;\hat{\theta}(\mathbf{1}))))\| = \|t(y_i) - \mathbb{E}_{\mathsf{y}\sim P_{\mathsf{y}|\mathsf{x}=x_i;\hat{\theta}(\mathbf{1})}}\left[t(\mathsf{y})\right]\|.$$

Moreover, $\bar{E}_n$ can be shown to serve as an upper bound on the gradient at the optimum $\hat{\theta}(\mathbf{1})$ (see App. B, App. C). In App. B, we further demonstrate how this term relates to the absolute training error in classification and regression problems. Specifically, as training error decreases, this term also diminishes. In the extreme case where $\ell(z_i,\hat{\theta}(\mathbf{1})) = 0$ for all $i \in [n]$, this term is exactly zero (see App. E). Thus, we expect the excess term in (10) to be small whenever the model's training loss is small. For the remaining terms in Lem. 1, the worst-case discrepancy between $\tilde{\theta}(w^n)$ and $\hat{\theta}(w^n)$ for all $i \in [n]$ is controlled by $g_{\max} \triangleq \max_{i\in[n]} g_i$. By Assump. 4 with $(s,r) = (0,1)$, $g_{\max}$ is finite.

Next, we present our main theorem, which establishes error bounds for the approximated inference objective $T(\cdot)$.

Theorem 1. *Suppose Assump. 1, Assump. 2, and Assump. 5-Assump. 7 hold. Let $\tilde{\theta}(w^n)$ be defined as in (9) for $w^n \in \mathscr{D}^{-i}$. Then,*

$$\|T(\hat{\theta}(w^n)) - T(\tilde{\theta}(w^n))\| \leq C_{T_1}\left(\frac{2QC_f^2\tilde{g}_i}{n^2\mu^2} + \frac{M\tilde{g}_i^2}{n^2\mu^3} + \frac{2\tilde{g}_i\tilde{C}_f\bar{E}_n}{n\mu^2}\right) + \frac{1}{2}C_{T_2}\left(\frac{2QC_f^2\tilde{g}_i}{n^2\mu^2} + \frac{M\tilde{g}_i^2}{n^2\mu^3} + \frac{2\tilde{g}_i\tilde{C}_f\bar{E}_n}{n\mu^2}\right)^2 \tag{11}$$

and,

$$\begin{aligned}\|T(\hat{\theta}(w^n)) - T(\hat{\theta}(\mathbf{1})) - \langle\nabla T(\hat{\theta}(\mathbf{1})), \tilde{\theta}(w^n) - \hat{\theta}(\mathbf{1})\rangle\| \\ \leq C_{T_1}\left(\frac{2QC_f^2\tilde{g}_i}{n^2\mu^2} + \frac{M\tilde{g}_i^2}{n^2\mu^3} + \frac{2\tilde{g}_i\tilde{C}_f\bar{E}_n}{n\mu^2}\right) + \frac{2C_{T_2}\tilde{g}_i^2}{n^2\mu^2}.\end{aligned} \tag{12}$$

Proof sketch. Both bounds follow from the smoothness properties of T (Assump. 6), combined with Lem. 1 and Lem. 2 from App. D. Full proof is provided in App. H. □

Th. 1 enables a systematic derivation of theoretical guarantees for FIM-based influence approximations across various application areas. Moreover, as discussed in [22, Sec. 3], for weight vectors $w^n = \mathscr{D}^{-i}$, we expect $\lim_{n\to\infty} g_{\max} = 0$. Consequently, whenever $\bar{E}_n \to 0$, Th. 1 ensures that $T(\tilde{\theta}(w^n))$ and the Taylor-series approximation (Equation (4) with $w^n \in \mathscr{D}^{-i}$) converge to $T(\hat{\theta}(w^n))$ for all $i \in [n]$. However, as we demonstrate in Sec. 5.1 and Sec. 5.2, in practice, $\tilde{\theta}(w^n)$ is often a good approximation of $\hat{\theta}(w^n)$ even when $\bar{E}_n$ is finite.

Next, we show that our framework provides guarantees in a unified manner, analogous to Prop. 1–Prop. 3, which establish Hessian-based guarantees for several tasks outlined in Sec. 2.

Corollary 1 (LOOCV)**.** *Suppose Assump. 1, Assump. 2, and Assump. 4-Assump. 7 hold with $(s,r) = \{(0,2),(0,3),(1,2),(1,3),(1,4)\}$. Let $T(\theta, \mathbf{1}^{n\setminus i}) = \frac{1}{n}\ell(z_i,\theta) \triangleq T_i(\theta)$. When $\tilde{\theta}(w^n)$ from Lem. 1 is used as a plug-in estimate for $w^n \in \mathscr{D}^{-i}$, the error in the approximate cross-validation estimate satisfies:*

$$\left|\sum_{i=1}^{n}\left(T_i(\tilde{\theta}(\mathbf{1}^{n\setminus i})) - T_i(\hat{\theta}(\mathbf{1}^{n\setminus i}))\right)\right| \leq O\left(\frac{MB_{03}}{\mu^3 n^2} + \frac{C_f^2 B_{02}}{\mu^2 n^2} + \frac{\tilde{C}_f\bar{E}_n B_{02}}{\mu^2 n}\right).$$

Corollary 2 (Machine Unlearning)**.** *Suppose Assump. 1, Assump. 2, Assump. 5, and Assump. 7 hold. Assume further that $\tilde{g}_i \leq G$ for all $i \in [n]$. Then, for the inference objective $T(\theta) = \theta$, we have:*

$$\|T(\tilde{\theta}(w^n)) - T(\hat{\theta}(w^n))\| \leq \frac{2QC_f^2 G}{n^2\mu^2} + \frac{MG^2}{n^2\mu^3} + \frac{2G\tilde{C}_f\bar{E}_n}{n\mu^2}, \quad \textit{for } w^n \in \mathscr{D}^{-i}.$$

Furthermore, the algorithm returning $\tilde{\theta}(w^n) + \zeta$ satisfies (ε,δ)-unlearning, where $\zeta \sim \mathcal{N}(0, c\mathbf{I})$ and:

$$c = \left(\frac{2QC_f^2 G}{n^2\mu^2} + \frac{MG^2}{n^2\mu^3} + \frac{2G\tilde{C}_f\bar{E}_n}{n\mu^2}\right)\frac{\sqrt{2\log(5/4\delta)}}{\varepsilon}.$$

Corollary 3 (Data Attribution)**.** *Suppose the assumptions of Th. 1 hold,* $T(\theta) = \ell(z_{\text{test}}, \theta) - \ell(z_{\text{test}}, \hat{\theta}(\mathbf{1}))$ *and* $C_\ell \triangleq \max_{i\in[n]} \tilde{g}_i$*. Then,*

$$|T(\hat{\theta}(\mathbf{1}^{n\setminus i})) - T(\tilde{\theta}(\mathbf{1}^{n\setminus i}))| \leq O\left(\frac{C_f^2 C_{T_1} C_\ell}{n^2\mu^2} + \frac{M C_{T_1} C_\ell^2}{n^2\mu^3} + \frac{C_{T_1}\tilde{C}_f \bar{E}_n C_\ell}{n\mu^2}\right),$$

$$|T(\hat{\theta}(\mathbf{1}^{n\setminus i})) - T(\hat{\theta}(\mathbf{1})) - \langle \nabla T(\hat{\theta}(\mathbf{1})), \tilde{\theta}(\mathbf{1}^{n\setminus i}) - \hat{\theta}(\mathbf{1})\rangle|$$
$$\leq O\left(\frac{C_f^2 C_{T_1} C_\ell}{n^2\mu^2} + \frac{M C_{T_1} C_\ell^2}{n^2\mu^3} + \frac{C_{T_2} C_\ell^2}{n^2\mu^2} + \frac{C_{T_1}\tilde{C}_f \bar{E}_n C_\ell}{n\mu^2}\right)$$

The proofs for these corollaries rely on applying Th. 1 for the settings described in Prop. 1 - Prop. 3 (see App. I). To further demonstrate the generality of our approach, we provide guarantees for the fairness assessment task described in Sec. 2, for which currently there is no theoretical analysis. The proof is in App. I.4.

Corollary 4 (Fairness Evaluation)**.** *Suppose Assump. 1, Assump. 2, and Assump. 5 - Assump. 7 hold. If* T *be given by* (2) *and* $C_\ell \triangleq \max_{i\in[n]} \tilde{g}_i$*. Then,*

$$|T(\hat{\theta}(\mathbf{1}^{n\setminus i})) - T(\tilde{\theta}(\mathbf{1}^{n\setminus i}))| \leq O\left(\frac{C_f^3 C_\ell}{n^2\mu^2} + \frac{M C_f C_\ell^2}{n^2\mu^3} + \frac{C_f \tilde{C}_f C_\ell \bar{E}_n}{n\mu^2}\right).$$

To the best of our knowledge, Corol. 1 - Corol. 4 provide the first theoretical guarantees for using the FIM in influence assessment tasks, offering a novel method with rigorous effectiveness proof. Additionally, our framework easily extends to other problems in machine learning and statistics beyond the specific applications discussed (e.g., data dropping [10]).

Remark 3 (The Non-Convex Setting). While many theoretical analyses of influence (e.g., [27]) assume a convex, differentiable loss, these assumptions often do not hold in practice. Nonetheless, influence functions remain widely used for influence assessment [27, 25]. Recent work [4] shows that a variant of Fisher influence corresponds to the minimizer of an approximation to the Proximal Bregman Response Function (PBRF). This finding helps explain the empirical usefulness of influence functions in more complex domains and illustrates how analyses grounded in convex assumptions can still offer valuable insights for non-convex scenarios. Our probabilistic framework extends these results by introducing $\tilde{\theta}(\mathbf{1}^{n\setminus i})$, which depends on $\tilde{\theta}^{\text{IJ,AF}}(\mathbf{1}^{n\setminus i})$ and can be computed efficiently. It further provides a theoretical justification for using the AFIF by establishing bounds on $\|\tilde{\theta}^{\text{IJ}}(\mathbf{1}^{n\setminus i}) - \tilde{\theta}(\mathbf{1}^{n\setminus i})\|$ under mild assumptions likely to hold locally (see App. J). These results support adopting AFIF over traditional Hessian-based methods. Moreover, while [4] focuses on $\pi(\theta) = \|\theta\|^2$, our framework readily accommodates non-differentiable regularizers. Since training models with general regularization (beyond L_2) is an increasingly popular method for adding robustness, feature sparsity, and interoperability to models (see [32, 33] and references therein), our approach gives a state-of-the-art tool for quantifying influence in these cases.

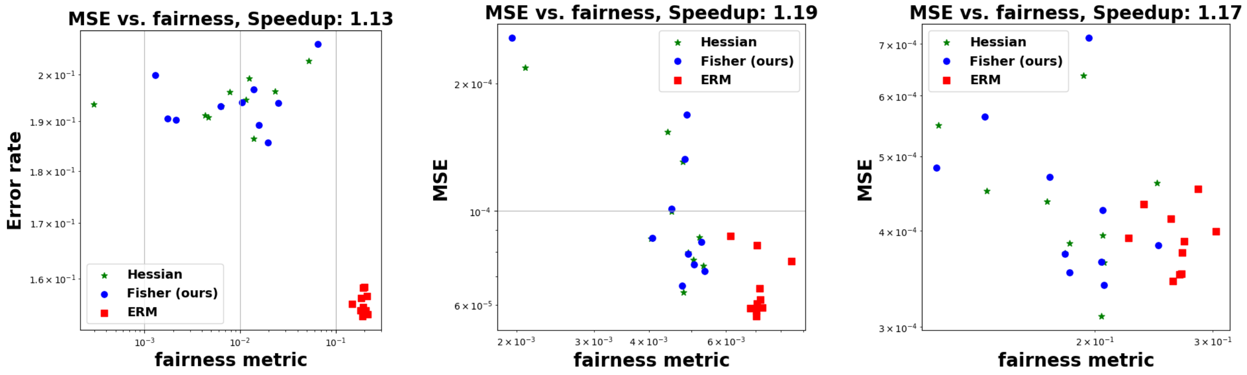

(a) Adult

(b) Insurance

(c) Crime

Figure 1: Model performance versus fairness metric for Fisher-based influence, Hessian-based influence, and the ERM solution from (1), evaluated on the Adult, Crime, and Insurance datasets using a two-layer classifier. Results are averaged over ten independent experiments. All cases demonstrate that the Fisher-based computations are faster than the Hessian-based computations yet still yield similar overall utility.

5 Experiments

We evaluate the utility of approximate Fisher influence through experiments on three different tasks. Both Fisher-based and Hessian-based influence functions are implemented within the same codebase, differing only in the automatic differentiation components used to compute (7) and (8). Detailed experimental procedures are provided in App. K. Our objective is to demonstrate the advantages of AFIF across different tasks by showing that, across a set of different classical influence measurement settings, it:

1. Achieves similar utility as the Hessian-based techniques
2. Has improved computational efficiency relative to the Hessian-based techniques.

We will further demonstrate the usefulness of our technique in a setting that involves a non-differentiable regularizer, demonstrating a novel method for measuring influence in these cases. The codebase to reproduce our experimental results is provided in https://github.com/omrilev1/Approximate-Fisher-Influence.

5.1 Fairness and Unlearning

In this set of experiments, we aim to identify and unlearn training points that negatively impact model fairness. To that end, we use three classical datasets from the fairness literature [45, 46, 41]: Adult, Crime, and Insurance datasets. For the Adult dataset, the goal is to classify whether a person's income is greater than 50, 000$, while keeping the classifier independent of the person's sex. For the crime dataset, the goal is to predict crime per population (which is a continuous variable), while keeping the regressor independent of race. For the insurance dataset, the goal is to predict medical expenses and make the regressor independent of sex. Fairness is assessed using the demographic parity metric for the adult dataset and using the χ^2 divergence for the crime and the insurance datasets. Our models are two-layer networks with SeLU activations, similar to the architectures from [20, 46, 41]. We used (2) and (3) as our inference objectives and calculated the influence for each training sample using the plug-in estimator from Th. 1. We then unlearned all training samples with positive influence by applying (9). Full experimental details are provided in App. K.

We measured the time required to compute influences and unlearn samples using both Fisher-based and Hessian-based calculations, reporting the model's performance (measured via classification accuracy for the adult dataset and MSE for the crime and insurance datasets) and estimated fairness (measured either via DP or via the χ^2 measure) after data removal. As shown in Fig. 1, both methods perform similarly, significantly improving fairness score without substantial performance loss, matching results from [41, 46]. However, the Fisher-based results are consistently faster relative to the Hessian-based approaches, demonstrating the computational efficiency of the Fisher-based influence. We give details of additional experiments in App. L.1, which show that the Hessian-based influence fails to improve the model's fairness and to maintain the same performance for different choices of hyperparameters, demonstrating potential instabilities without proper hyperparameter tuning. Additionally, the error rates and MSE of the ERM minimizers are strictly positive, corresponding to a finite $\bar{E}_n$. Nevertheless, the AFIF effectively identifies and unlearns samples that negatively impact fairness, demonstrating its usefulness when $\bar{E}_n$ is finite.

5.2 Cross-Validation

In our second example, we establish our method's computational advantage and demonstrate the improved stability of the approximate Fisher influence, as described in our prior remark about computational stability, when used to approximate cross-validation. To that end, we used the same two-layer model used in Sec. 5.1 for the adult dataset, increased the width of the hidden layer to 30000, and have trained the model with a weight decay of 10^{-8}. We thus expect the model's Hessian to be ill-conditioned, preventing (5) from working without a proper regularization. Our goal was to estimate the test loss of the model as a function of the number of epochs using CV. To the best of our knowledge, this is the first work to apply the FIM to approximate CV. To reduce the computational complexity of the LOOCV, we used a leave-k-out CV with k set to 6000, corresponding to ∼20% of the trainset, and then averaged five different estimates to generate the final value (see App. K.4 for further details). Fig. 2 reports the test loss, estimated loss, and average computation time (to generate an estimate based on the five different folds) for each method. The results show that the Hessian-based method fails to converge to the correct estimate, while the Fisher-based method follows the test loss trend, demonstrating potential instabilities of using (5). Additional experiments in App. L.2 confirm this behavior across other hyperparameter choices. Moreover, Fisher-based CV requires ∼50% less time than the Hessian-based estimate.

5.3 Data Attribution

To demonstrate the effectiveness of the AFIF in a high-dimensional non-convex setting, we attribute test sample predictions to training data using two popular neural network

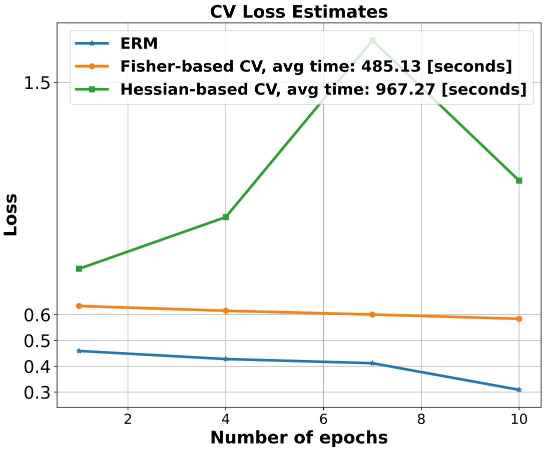

Figure 2: Test loss and CV estimators for Fisher and Hessian-based influence on the Adult dataset using a two-layer classifier, averaged over five folds. Fisher calculations are approximately twice as fast as Hessian computations and Hessian estimates are highly unstable, yielding invalid loss estimates.

architectures: the ResNet18 [26] and a model comprised of three convolutional layers and two fully connected layers, on a subset of CIFAR-10 [29], focusing on the "plane" and "car" classes (see App. K). We calculated the influence of training examples on the 30 test instances with the highest test loss. Fig. 3, Fig. 4 and Fig. 5 present the three images with the highest and the lowest influence scores and the computation times for both cases. Both methods identified the same influential training samples, with a maximal discrepancy between influence scores, which was less than 20% of the maximal influence value. However, the AFIF calculations were faster than the Hessian-based calculations in both simulated cases.

6 Concluding Remarks

In this work, we introduced the AFIF, a novel method for quantifying influence in machine learning models. By using the FIM instead of the Hessian, we demonstrate how our technique is fundamentally faster than existing influence function baselines yet provides similar error guarantees across a set of tasks. Moreover, our framework extends the applicability of influence measurement to a broader range of scenarios—including those involving non-differentiable regularizers. We demonstrated the computational efficiency of AFIF relative to traditional Hessian-based techniques and its usefulness in providing reliable influence estimates across a set of tasks in a set of empirical evaluations.

Generalizing our analysis to more complex, real-world influence measurement methods that are based on the FIM and currently lack rigorous theoretical support (for example, techniques based on the Kronecker-Factored FIM [12]) is a promising future research direction, that will open the door to systematically determining when and how such methods can be most effectively applied across diverse tasks. Moreover, developing computationally efficient variants

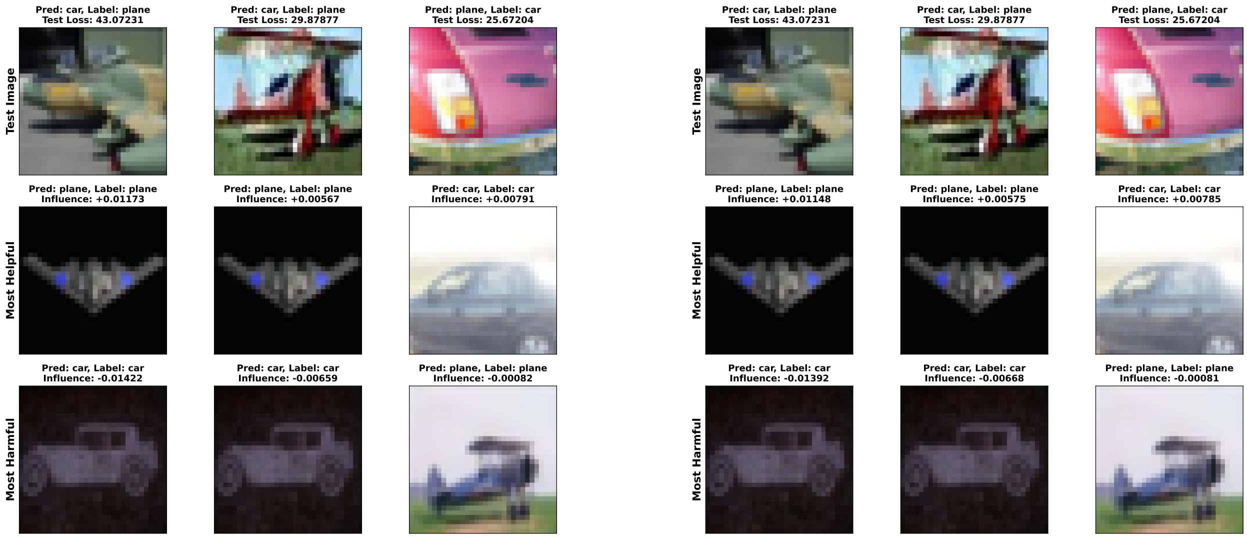

(a) Fisher

(b) Hessian

Figure 3: Most and least influential images on a subset of CIFAR10 when using a simple CNN architecture.

of higher-order influence measurement techniques such as those explored in [21, 7] (see also the discussion in [27]) by utilizing the underlying statistical nature of the optimization problem is another future research direction, that is currently under investigation.

References

[1] Naman Agarwal, Brian Bullins, and Elad Hazan. Second-order stochastic optimization for machine learning in linear time. *J. Mach. Learn. Res. (JMLR)*, 18(116):1–40, 2017.

[2] Shun-ichi Amari. *Information geometry and its applications*, volume 194. Springer, 2016.

[3] Shun-Ichi Amari and Scott C Douglas. Why natural gradient? In *Proc. IEEE Int. Conf. Acoust. Speech and Sig. Proc. (ICASSP)*, volume 2, pages 1213–1216. IEEE, 1998.

[4] Juhan Bae, Nathan Ng, Alston Lo, Marzyeh Ghassemi, and Roger B Grosse. If influence functions are the answer, then what is the question? In *Adv. Neural Inf. Process. Syst. (NeurIPS)*, volume 35, pages 17953–17967, 2022.

[5] Arindam Banerjee, Srujana Merugu, Inderjit S Dhillon, and Joydeep Ghosh. Clustering with Bregman divergences. *J. Mach. Learn. Res.*, 6(Oct):1705–1749, 2005.

[6] Samyadeep Basu, Philip Pope, and Soheil Feizi. Influence functions in deep learning are fragile. *arXiv preprint arXiv:2006.14651*, 2020.

[7] Samyadeep Basu, Xuchen You, and Soheil Feizi. On second-order group influence functions for black-box predictions. In *Proc. Int. Conf. Mach. Learn. (ICML)*, pages 715–724. PMLR, 2020.

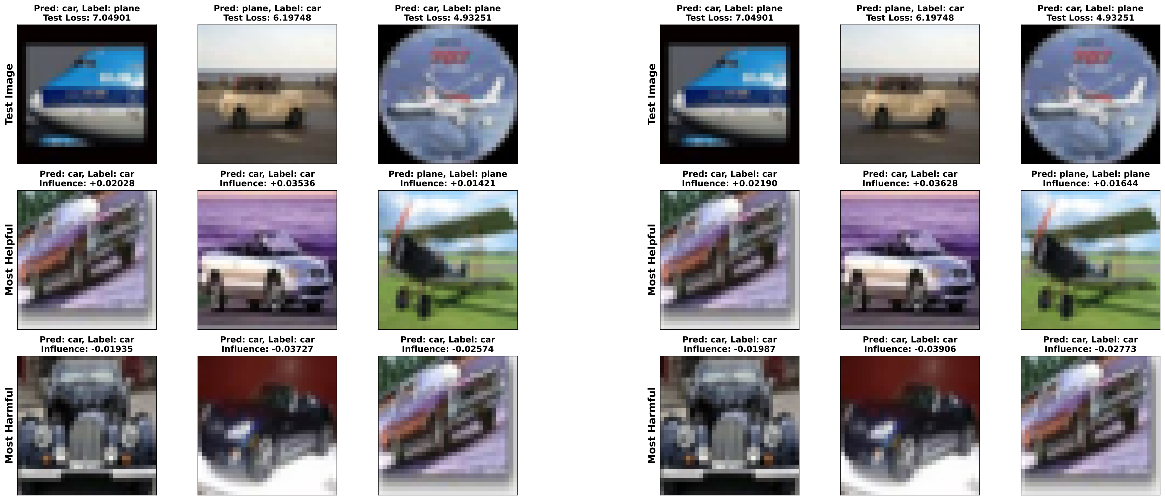

(a) Fisher

(b) Hessian

Figure 4: Most and least influential images on a subset of CIFAR10 when using the ResNet18 architecture.

[8] Ahmad Beirami, Meisam Razaviyayn, Shahin Shahrampour, and Vahid Tarokh. On optimal generalizability in parametric learning. *Adv. Neural Inf. Process. Syst. (NeurIPS)*, 30, 2017.

[9] James Bradbury, Roy Frostig, Peter Hawkins, Matthew James Johnson, Chris Leary, Dougal Maclaurin, George Necula, Adam Paszke, Jake VanderPlas, Skye Wanderman-Milne, et al. JAX: composable transformations of Python+ NumPy programs. 2018.

[10] Tamara Broderick, Ryan Giordano, and Rachael Meager. An automatic finite-sample robustness metric: when can dropping a little data make a big difference? *arXiv preprint arXiv:2011.14999*, 2020.

[11] Yinzhi Cao and Junfeng Yang. Towards making systems forget with machine unlearning. In *IEEE Symp. Secur. Privacy.*, pages 463–480, 2015. doi: 10.1109/SP.2015.35.

[12] Sang Keun Choe, Hwijeen Ahn, Juhan Bae, Kewen Zhao, Minsoo Kang, Youngseog Chung, Adithya Pratapa, Willie Neiswanger, Emma Strubell, Teruko Mitamura, et al. What is your data worth to gpt? llm-scale data valuation with influence functions. *arXiv preprint arXiv:2405.13954*, 2024.

[13] R Dennis Cook and Sanford Weisberg. Characterizations of an empirical influence function for detecting influential cases in regression. *Technometrics*, 22(4):495–508, 1980.

[14] Mathieu Dagréou, Pierre Ablin, Samuel Vaiter, and Thomas Moreau. How to compute Hessian-vector products? In *ICLR Blogposts 2024*, 2024. URL https://iclr-blogposts.github.io/2024/blog/bench-hvp/. https://iclr-blogposts.github.io/2024/blog/bench-hvp/.

[15] Santanu Das, Jatin Batra, and Piyush Srivastava. A unified law of robustness for Bregman divergence losses. *arXiv preprint arXiv:2405.16639*, 2024.

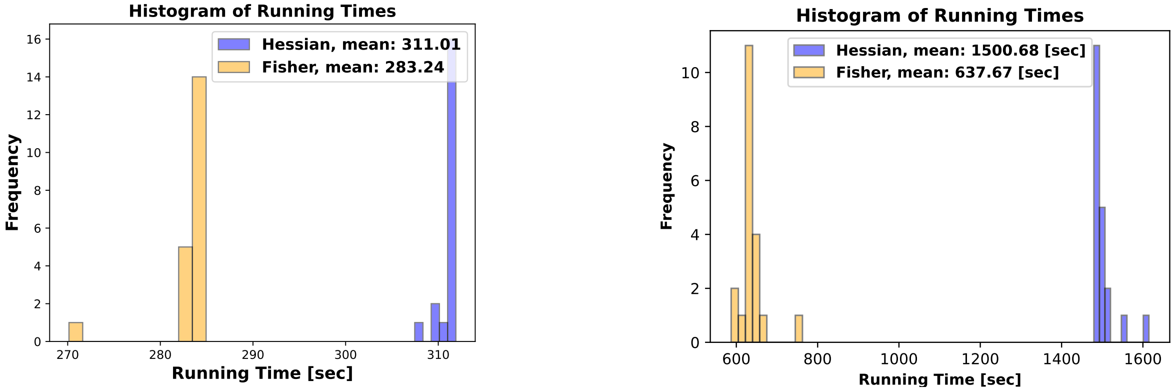

(a) CNN

(b) ResNet 18

Figure 5: Running times for Fisher-based and Hessian-based influence function when calculated on a subset of CIFAR10 classified using ResNet18 and a simple three-layer CNN. In both cases, Fisher-based influence significantly accelerates the influence calculation.

[16] DeepSpeed. Deepspeed tutorials: Flops profiler. https://www.deepspeed.ai/tutorials/flops-profiler/#flops-measurement, 2024. Accessed: 2024-09-17.

[17] Dheeru Dua, Casey Graff, et al. UCI machine learning repository, 2017. *URL http://archive. ics. uci. edu/ml*, 7(1):62, 2017.

[18] Cynthia Dwork, Aaron Roth, et al. The algorithmic foundations of differential privacy. *Foundations and Trends® in Theoretical Computer Science*, 9(3–4):211–407, 2014.

[19] Seymour Geisser. The predictive sample reuse method with applications. *J. Am. Stat. Assoc. (JASA)*, 70(350):320–328, 1975.

[20] Soumya Ghosh, Prasanna Sattigeri, Inkit Padhi, Manish Nagireddy, and Jie Chen. Influence based approaches to algorithmic fairness: A closer look. In *XAI in Action: Past, Present, and Future Applications*, 2023.

[21] Ryan Giordano, Michael I Jordan, and Tamara Broderick. A higher-order swiss army infinitesimal jackknife. *arXiv preprint arXiv:1907.12116*, 2019.

[22] Ryan Giordano, William Stephenson, Runjing Liu, Michael Jordan, and Tamara Broderick. A swiss army infinitesimal jackknife. In *Int. Conf. Artif. Intell. Stat. (AISTATS)*, pages 1139–1147. PMLR, 2019.

[23] Roger Grosse, Juhan Bae, Cem Anil, Nelson Elhage, Alex Tamkin, Amirhossein Tajdini, Benoit Steiner, Dustin Li, Esin Durmus, Ethan Perez, et al. Studying large language model generalization with influence functions. *arXiv preprint arXiv:2308.03296*, 2023.

[24] Han Guo, Nazneen Fatema Rajani, Peter Hase, Mohit Bansal, and Caiming Xiong. Fastif: Scalable influence functions for efficient model interpretation and debugging. *arXiv preprint arXiv:2012.15781*, 2020.

[25] Xiaochuang Han, Byron C Wallace, and Yulia Tsvetkov. Explaining black box predictions

and unveiling data artifacts through influence functions. *arXiv preprint arXiv:2005.06676*, 2020.

[26] Kaiming He, Xiangyu Zhang, Shaoqing Ren, and Jian Sun. Deep residual learning for image recognition. In *Proc. IEEE Conf. Comput. Vis. Pattern Recognit.*, pages 770–778, 2016.

[27] Pang Wei Koh and Percy Liang. Understanding black-box predictions via influence functions. In *Proc. Int. Conf. Mach. Learn. (ICML)*, pages 1885–1894. PMLR, 2017.

[28] Pang Wei W Koh, Kai-Siang Ang, Hubert Teo, and Percy S Liang. On the accuracy of influence functions for measuring group effects. *Adv. Neural Inf. Process. Syst. (NeurIPS)*, 32, 2019.

[29] Alex Krizhevsky and Geoffrey Hinton. Learning multiple layers of features from tiny images. Technical report, University of Torontro, ON, Canada, 2009. URL https://www.cs.toronto.edu/~kriz/learning-features-2009-TR.pdf.

[30] Frederik Kunstner, Philipp Hennig, and Lukas Balles. Limitations of the empirical Fisher approximation for natural gradient descent. In *Adv. Neural Inf. Process. Syst. (NeurIPS)*, volume 32, 2019.

[31] Brett Lantz. *Machine learning with R: expert techniques for predictive modeling.* Packt publishing ltd, 2019.

[32] Ismael Lemhadri, Feng Ruan, Louis Abraham, and Robert Tibshirani. Lassonet: A neural network with feature sparsity. *J. Mach. Learn. Res.*, 22(127):1–29, 2021.

[33] Gen Li, Yuantao Gu, and Jie Ding. *ell*_1 regularization in two-layer neural networks. *IEEE Signal Processing Letters*, 29:135–139, 2021.

[34] Ilya Loshchilov, Frank Hutter, et al. Fixing weight decay regularization in adam. *arXiv preprint arXiv:1711.05101*, 5, 2017.

[35] James Martens. New insights and perspectives on the natural gradient method. *J. Mach. Learn. Res. (JMLR)*, 21(1):5776–5851, 2020.

[36] Jérémie Mary, Clément Calauzenes, and Noureddine El Karoui. Fairness-aware learning for continuous attributes and treatments. In *Proc. Int. Conf. Mach. Learn. (ICML)*, pages 4382–4391. PMLR, 2019.

[37] Yurii Nesterov. *Introductory lectures on convex optimization: A basic course*, volume 87. Springer Science & Business Media, 2013.

[38] Adam Paszke, Sam Gross, Francisco Massa, Adam Lerer, James Bradbury, Gregory Chanan, Trevor Killeen, Zeming Lin, Natalia Gimelshein, Luca Antiga, et al. Pytorch: an imperative style, high-performance deep learning library. In *Adv. Neural Inf. Process. Syst. (NeurIPS)*, volume 32, 2019.

[39] Mert Pilanci and Tolga Ergen. Neural networks are convex regularizers: Exact polynomial-time convex optimization formulations for two-layer networks. In *Proc. Int. Conf. Mach. Learn. (ICML)*, pages 7695–7705. PMLR, 2020.

[40] Michael Redmond and Alok Baveja. A data-driven software tool for enabling cooperative information sharing among police departments. *European Journal of Operational Research*, 141(3):660–678, 2002.

[41] Prasanna Sattigeri, Soumya Ghosh, Inkit Padhi, Pierre Dognin, and Kush R Varshney. Fair infinitesimal jackknife: Mitigating the influence of biased training data points without refitting. *Adv. Neural Inf. Process. Syst. (NeurIPS)*, 35:35894–35906, 2022.

[42] Andrea Schioppa, Polina Zablotskaia, David Vilar, and Artem Sokolov. Scaling up influence functions. In *Proceedings of the AAAI Conference on Artificial Intelligence*, volume 36, pages 8179–8186, 2022.

[43] Nicol N. Schraudolph. Fast curvature matrix-vector products for second-order gradient descent. *Neural Computation*, 14(7):1723–1738, 2002.

[44] Ayush Sekhari, Jayadev Acharya, Gautam Kamath, and Ananda Theertha Suresh. Remember what you want to forget: Algorithms for machine unlearning. In *Adv. Neural Inf. Process. Syst. (NeurIPS)*, volume 34, pages 18075–18086, 2021.

[45] Abhin Shah, Yuheng Bu, Joshua K Lee, Subhro Das, Rameswar Panda, Prasanna Sattigeri, and Gregory W Wornell. Selective regression under fairness criteria. In *Proc. Int. Conf. Mach. Learn. (ICML)*, pages 19598–19615. PMLR, 2022.

[46] Abhin Shah, Maohao Shen, Jongha Jon Ryu, Subhro Das, Prasanna Sattigeri, Yuheng Bu, and Gregory W Wornell. Group fairness with uncertain sensitive attributes. In *Proc. IEEE Int. Symp. on Inf. Theory (ISIT)*, pages 208–213. IEEE, 2024.

[47] Sidak Pal Singh and Dan Alistarh. Woodfisher: Efficient second-order approximation for neural network compression. *Adv. Neural Inf. Process. Syst. (NeurIPS)*, 33:18098–18109, 2020.

[48] M. Stone. Cross-Validatory Choice and Assessment of Statistical Predictions. *Journal of the Royal Statistical Society: Series B (Methodological)*, 36(2):111–133, 12 1974.

[49] Vinith Suriyakumar and Ashia C. Wilson. Algorithms that approximate data removal: New results and limitations. In *Adv. Neural Inf. Process. Syst. (NeurIPS)*, volume 35, pages 18892–18903, 2022.

[50] Martin J Wainwright, Michael I Jordan, et al. Graphical models, exponential families, and variational inference. *Foundations and Trends® in Machine Learning*, 1(1–2):1–305, 2008.

[51] Ashia Wilson, Maximilian Kasy, and Lester Mackey. Approximate cross-validation: guarantees for model assessment and selection. In *Int. Conf. Artif. Intell. Stat. (AISTATS)*, pages 4530–4540. PMLR, 2020.

[52] Jie Xu, Zihan Wu, Cong Wang, and Xiaohua Jia. Machine unlearning: Solutions and challenges. *IEEE Trans. Emerg. Top. Comput. Intell.*, 2024.

[53] Emi Zeger and Mert Pilanci. Unveiling hidden convexity in deep learning: A sparse signal processing perspective.

Contents of Appendix

A Definitions and Useful Lemmas

The manuscript uses the next classical definitions from the convex optimization theory [37].

Definition 1 (Matrix Operator-Norm)**.** For any matrix $\mathbf{A}$ we define its *operator-norm* by $\|\mathbf{A}\|_{\mathrm{op}} \triangleq \sup_{v\in\mathbb{R}^d:\|v\|\neq 0} \|\mathbf{A}v\| / \|v\|$

Definition 2 (Strong convexity)**.** Let $\beta > 0$. A function $f(\cdot)$ is β-strongly convex if and only if

$$f(y) \geq f(x) + \nabla^\top f(x)(y-x) + \frac{\beta}{2}\|x-y\|^2, \ \forall(x,y) \in \mathrm{dom}(f)$$

Definition 3 (Lipschitz)**.** A function $f(\cdot)$ is C-Lipschitz if

$$\|f(x) - f(y)\| \leq C\|x-y\|, \ \forall(x,y) \in \mathrm{dom}(f).$$

In that case, C is called the Lipschitz constant of f and is denoted by $C \triangleq \mathrm{Lip}(f(x))$.

Definition 4 (Smooth)**.** If $f(\cdot)$ is differentiable, then $f(\cdot)$ is K-smooth if

$$\|\nabla f(x) - \nabla f(y)\| \leq K\|x-y\|, \ \forall(x,y) \in \mathrm{dom}(f).$$

In that case, K is called the gradient-Lipschitz constant of f and is denoted by $C \triangleq \mathrm{Lip}_1(f(x))$.

Definition 5 (Lipschitz-Hessian)**.** If $f(\cdot)$ is twice differentiable, then $f(\cdot)$ is M-Lipschitz Hessian if

$$\left\|\nabla^2 f(x) - \nabla^2 f(y)\right\|_{\mathrm{op}} \leq M\|x-y\|, \ \forall(x,y) \in \mathrm{dom}(f)$$

In that case, M is called the Lipschitz-Hessian constant of f and is denoted by $M \triangleq \mathrm{Lip}_2(f(x))$.

Throughout the manuscript, we will further make use of the next connections between Lipschitz coefficients and gradient bounds for differentiable functions.

Corollary 5 ([37])**.** *Let $f(x)$ be a differentiable function $\forall x \in$ dom(f). Then, $f(x)$ is C-Lipschitz if and only if*

$$\|\nabla f(x)\| \leq C, \ \forall x \in dom(f).$$

If $f(x)$ is twice-differentiable $\forall x \in dom(f)$ then $f(x)$ is K-smooth if and only if

$$\|\nabla^2 f(x)\|_{\mathrm{op}} \leq K, \forall x \in dom(f).$$

B Example for Losses From an Exponential Family

We now present a few examples of commonly used loss functions in machine learning that can be viewed as the negative log-likelihood of an exponential-family model. Specifically, let

$$\ell\big(y, f(x;\theta)\big) = -\log P\big(y \mid f(x;\theta)\big),$$

where $P(y \mid f(x;\theta))$ belongs to a (discrete) exponential family. Throughout this paper, we adopt the following form of an exponential family:

$$\log P\big(y \mid f(x;\theta)\big) = f(x;\theta)^{\top} t(y) - \log\Bigg(\sum_{\tilde{y}=1}^{|\mathcal{Y}|} \exp\big\{ f(x;\theta)^{\top} t(\tilde{y})\big\}\Bigg) \ + \ \beta(y), \tag{13}$$

where $t(y)$ are the *natural statistics* and $f(x;\theta)$ are the *natural parameters*.[5] The term $\beta(y)$ depends only on y (thus does not affect parameter learning) and ensures proper normalization. Below, we illustrate two popular examples of loss functions (see also [35, Sec. 9.2]) that arise naturally from this exponential-family framework.

1. **Cross-Entropy Loss.** A standard approach in multi-class classification over $|\mathcal{Y}|$ classes is the softmax parameterization:

$$\log P\big(y \mid f(x;\theta)\big) = \big(f(x;\theta)\big)_y - \log\Bigg(\sum_{\tilde{y}=1}^{|\mathcal{Y}|} \exp\big\{\big(f(x;\theta)\big)_{\tilde{y}}\big\}\Bigg), \quad y, \tilde{y} \in \{1, \dots, |\mathcal{Y}|\}.$$

Here, $f(x;\theta)$ is a vector of length $|\mathcal{Y}|$. By defining e_y as the one-hot vector with a 1 in the y-th entry and 0 elsewhere, we see that

$$\log P\big(y \mid f(x;\theta)\big) = f(x;\theta)^{\top} e_y - \log\Bigg(\sum_{\tilde{y}=1}^{|\mathcal{Y}|} \exp\{f(x;\theta)^{\top} e_{\tilde{y}}\}\Bigg),$$

thus matching (13) with natural statistics $t(y) = e_y$ and natural parameters $f(x;\theta)$. The corresponding loss,

$$\ell\big(y, f(x;\theta)\big) = -\log P\big(y \mid f(x;\theta)\big),$$

is the well-known cross-entropy.

2. **Mean Squared Error (MSE).** In a regression setting with a continuous target $y \in \mathbb{R}$, a unit-variance Gaussian model with mean $\mu = f(x;\theta)$ leads to

$$\log P\big(y \mid f(x;\theta)\big) = -\frac{1}{2}\big(y - f(x;\theta)\big)^2 = f(x;\theta)\, y - \frac{y^2}{2} - \frac{\big(f(x;\theta)\big)^2}{2}.$$

Comparing with (13), this corresponds to an exponential family whose natural statistics are $\big(y, y^2\big)$ and whose natural parameters are $\big(f(x;\theta), -\frac{1}{2}\big)$. The negative log-likelihood here,

$$\ell\big(y, f(x;\theta)\big) = -\log P\big(y \mid f(x;\theta)\big) = \frac{1}{2}\big(y - f(x;\theta)\big)^2 \ + \ \text{(constant)},$$

is precisely the mean squared error (MSE) loss up to an additive constant.

[5] The above is a discrete version; for continuous $\mathcal{Y}$, one replaces the sum with an integral.

B.1 Bregman Losses

Following [5, Thm. 4], whenever the representation $P(y|f(x;\theta))$ correspond to a regular exponential family, then the loss $-\log(P(y|f(x;\theta)))$ can be expressed as

$$-\log(P(y|f_\theta(x))) = d_\varphi(t(y), \mu(f_\theta(x))) + \log(b_\varphi(t(y))) + C$$

where $\mu(f_\theta(x)) = \mathbb{E}\left[t(y)\right]$ is the expected value of $t(y)$ using the underlying exponential family distribution, $d_\varphi(\cdot,\cdot)$ is a Bregman divergence and C is a constant. As shown by [5, Table 1] (see also [15]), this result implies that many classical losses in machine learning, including cross-entropy and mean squared error, can be viewed as special cases of Bregman divergences, and further belong to the exponential family characterization discussed in our work.

B.2 Properties of the Cross-Entropy and MSE Losses

We now demonstrate how the assumptions on loss minimization, Hessian boundedness, and simplified second-order gradients follow for the two loss functions introduced above.

1. **Cross-Entropy Loss.** Recall the parameterization

$$\log P\big(y \mid f(x;\theta)\big) = (f(x;\theta))_y - \log\Big(\sum_{\tilde{y}\in\mathcal{Y}} \exp\{(f(x;\theta))_{\tilde{y}}\}\Big),$$

and let

$$\ell\big(y, f(x;\theta)\big) = -\log P\big(y \mid f(x;\theta)\big) = \log\Big(\sum_{\tilde{y}\in\mathcal{Y}} \exp\{(f(x;\theta))_{\tilde{y}}\}\Big) - (f(x;\theta))_y.$$

We focus first on the gradient of the *log-probability* itself (sometimes termed the "score function"):

$$\begin{aligned}\nabla_f \log P\big(y \mid f(x;\theta)\big) &= \nabla_f\Big[(f(x;\theta))_y - \log\big(\sum_{\tilde{y}\in\mathcal{Y}} \exp\{(f(x;\theta))_{\tilde{y}}\}\big)\Big]\\ &= e_y - \mathrm{softmax}\big(f(x;\theta)\big),\end{aligned}$$

where e_y is the one-hot vector selecting entry y, and $\mathrm{softmax}\big(f(x;\theta)\big)$ is the vector of class probabilities assigned by the model.

Zero Gradients Under Perfect Prediction. For any training example (x_i, y_i), if the model classifies it with perfect confidence, i.e.

$$\big(\mathrm{softmax}(f(x_i;\hat{\theta}(\mathbf{1})))\big)_{y_i} = 1,$$

then $\nabla_f \log P\big(y_i \mid f(x_i;\hat{\theta}(\mathbf{1}))\big) = 0$. Consequently, if the model perfectly predicts *all* training labels, then all these gradients vanish simultaneously.

Bounded Hessian. Next, we show that the second derivative (the Hessian) of $\log P\big(y \mid f(x;\theta)\big)$ with respect to f is bounded in norm. From the above,

$$\nabla_f \log P\big(y \mid f(x;\theta)\big) = e_y - \mathrm{softmax}\big(f(x;\theta)\big),$$

so taking another derivative,

$$\nabla_f^2 \log P\big(y \mid f(x;\theta)\big) = -\,\nabla_f \big[\mathrm{softmax}(f(x;\theta))\big].$$

Denote $\mathbf{C}_f \triangleq \nabla_f\big[\mathrm{softmax}(f(x;\theta))\big]$. By the well-known derivative of softmax, the (i,j)th entry of $\mathbf{C}_f$ is

$$(\mathbf{C}_f)_{ij} = \frac{\partial}{\partial\big(f(x;\theta)\big)_j}\Big[\mathrm{softmax}(f(x;\theta))_i\Big] = \mathrm{softmax}(f(x;\theta))_i\left[\delta_{ij} - \mathrm{softmax}(f(x;\theta))_j\right],$$

which implies:

$$\begin{aligned}(\mathbf{C}_f)_{ii} &= \mathrm{softmax}(f(x;\theta))_i\big[1 - \mathrm{softmax}(f(x;\theta))_i\big],\\ (\mathbf{C}_f)_{ij} &= -\mathrm{softmax}(f(x;\theta))_i \mathrm{softmax}(f(x;\theta))_j \quad (i \neq j).\end{aligned}$$

Because each $\mathrm{softmax}(f(x;\theta))_i \in [0,1]$, the entries of $\mathbf{C}_f$ lie in $[-1,1]$, and indeed one can show $\|\mathbf{C}_f\|$ is bounded by a constant (depending only on $|\mathcal{Y}|$, not on the dimension of the parameters). Hence $\nabla_f^2 \log P\big(y \mid f(x;\theta)\big) = -\mathbf{C}_f$ is also bounded in norm, establishing the desired Hessian bound.

2. **Mean Squared Error (MSE).** For the MSE loss arising from a unit-variance Gaussian,

$$\log P\big(y \mid f(x;\theta)\big) = -\frac{1}{2}\left[y - f(x;\theta)\right]^2,$$

the gradient with respect to $f(x;\theta)$ is simply

$$\nabla_f \, \log P\big(y \mid f(x;\theta)\big) = y - f(x;\theta).$$

Hence, if at $\hat{\theta}(\mathbf{1})$ the model predictions perfectly match all responses, this gradient becomes zero for each training pair, indicating perfect minimization of the training error.

Bounded Hessian. Since

$$\nabla_f^2 \, \log P\big(y \mid f(x;\theta)\big) = -\,\nabla_f^2\left[\frac{1}{2}\,(y - f(x;\theta))^2\right] = -\,(-\mathbf{I}_d) = \mathbf{I}_d,$$

the Hessian with respect to f is simply the identity (for the one-dimensional f). Its norm is therefore trivially bounded by 1, and it does not depend on the dimension d of the parameters in θ. Moreover, the Hessian can be evaluated with no complicated operations—just the constant identity matrix at each sample.

C Gradient Bound for Minimizing Losses With Exponential Family Structure

Given a training set $\{(x_i, y_i)\}_{i=1}^n$ and the loss function (13) we derive gradient of the empirical risk (1) which we aim to minimize. To that end, we note that

$$\begin{aligned}
n\nabla_\theta L(\mathscr{D}, \theta, \mathbf{1}) &= \nabla_\theta \left(\sum_{i=1}^n f^\top(x_i;\theta)t(y_i) - \log\left(\sum_{\tilde{y}\in\mathcal{Y}} \exp\{f^\top(x_i;\theta)t(\tilde{y})\} \right) + \beta(y_i) \right) \\
&= \sum_{i=1}^n \left(\nabla_\theta^\top f(x_i;\theta)t(y_i) - \frac{\sum_{\tilde{y}\in\mathcal{Y}} \nabla^\top f(x_i;\theta)t(\tilde{y})\exp\{f^\top(x_i;\theta)t(\tilde{y})\}}{\sum_{\tilde{y}_1\in\mathcal{Y}} \exp\{f^\top(x_i;\theta)t(\tilde{y}_1)\}} \right) \\
&= \sum_{i=1}^n \nabla_\theta^\top f(x_i;\theta) \left(t(y_i) - \frac{\sum_{\tilde{y}\in\mathcal{Y}} t(\tilde{y})\exp\{f^\top(x_i;\theta)t(\tilde{y})\}}{\sum_{\tilde{y}_1\in\mathcal{Y}} \exp\{f^\top(x_i;\theta)t(\tilde{y}_1)\}} \right) \\
&= \sum_{i=1}^n \nabla_\theta^\top f(x_i;\theta)(t(y_i) - \mathbb{E}_{\mathsf{y}\sim P_{\mathsf{y}|\mathsf{x}=x_i;\theta}}[t(\mathsf{y})])
\end{aligned}$$

and the norm of this gradient is upper bounded by

$$n\left\|\nabla_\theta L(\mathscr{D}, \theta, \mathbf{1})\right\| \leq \sum_{i=1}^n \left\|\nabla_\theta f(x_i;\theta)\right\| \left\|t(y_i) - \mathbb{E}_{\mathsf{y}\sim P_{\mathsf{y}|\mathsf{x}=x_i;\theta}}[t(\mathsf{y})]\right\|$$

Thus, whenever the features are Lipschitz, we have

$$\left\|\nabla_\theta L(\mathscr{D}, \theta, \mathbf{1})\right\| \leq \frac{C_f}{n} \sum_{i=1}^n \left\|t(y_i) - \mathbb{E}_{\mathsf{y}\sim P_{\mathsf{y}|\mathsf{x}=x_i;\theta}}[t(\mathsf{y})]\right\|$$

and we expect this upper bound to be small at the minimizer $\theta = \hat{\theta}(\mathbf{1})$.

D Proof of Closeness of $\hat{\theta}(\mathbf{1})$ and $\hat{\theta}(\mathbf{1}^{n\setminus i})$

We will use the next lemma throughout our proofs.

Lemma 2. *Let $\hat{\theta}(\mathbf{1}^{n\setminus i})$ defined as in (1) and let $\frac{1}{n}\ell(z_i, \theta)$ be a differentiable function in θ for any $z_i \in \mathscr{D}$ and $\frac{1}{n}\ell(z_i, \theta) + \lambda\pi(\theta)$ be a μ-strongly convex function in θ for any $z_i \in \mathscr{D}$. Then, $\forall i \in [n]$*

$$\|\hat{\theta}(\mathbf{1}^{n\setminus i}) - \hat{\theta}(\mathbf{1})\| \leq \frac{2}{\mu} \cdot \max_{i\in[n]} \left\| \frac{1}{n}\nabla_\theta \ell(z_i, \hat{\theta}(\mathbf{1})) \right\|$$

Proof. Similarly to the developments from [51, App. B.1], we get that

$$
\begin{aligned}
\|\hat{\theta}(\mathbf{1})-\hat{\theta}(\mathbf{1}^{n\setminus i})\|^2 &\leq \frac{2}{\mu}|(\hat{\theta}(\mathbf{1})-\hat{\theta}(\mathbf{1}^{n\setminus i}))^\top(\nabla_\theta(L(\mathscr{D},\hat{\theta}(\mathbf{1}),\lambda,\mathbf{1}^{n\setminus i})-L(\mathscr{D},\hat{\theta}(\mathbf{1}),\lambda,\mathbf{1})))| \\
&\leq \frac{2}{\mu n}|(\hat{\theta}(\mathbf{1})-\hat{\theta}(\mathbf{1}^{n\setminus i}))^\top\nabla_\theta\ell(z_i,\hat{\theta}(\mathbf{1}))| \\
&\leq \frac{2}{\mu n}\|\hat{\theta}(\mathbf{1})-\hat{\theta}(\mathbf{1}^{n\setminus i})\|\|\nabla_\theta\ell(z_i,\hat{\theta}(\mathbf{1}))\|
\end{aligned}
$$

where all the steps are by Cauchy-Schwartz inequality. The proof follows by maximizing over i. □

We note that whenever $\frac{1}{n}\ell(z_i,\theta)$ is Lipschitz, the upper bound is finite. Moreover, since we normalize by n, the bound will go to zero with n whenever the gradient grows as $o(n)$, as is usually the case in many popular machine learning problems (see [22, Sec. 3]). We further note that under a more restrictive assumption that the $\ell(z_i,\theta)$ are Lipschitz then the bound is given by $\frac{2\tilde{C}}{\mu n}$ for $\tilde{C}=\max_{i\in[n]}\|\nabla_\theta\ell(z_i,\hat{\theta}(\mathbf{1}))\|$ and $\tilde{C}<\infty$.

E Proof of Lem. 1

The proof uses the following lemma from [51]:

Lemma 3 (Optimizer Comparison, [51]). *Let*

$$
x_{\varphi_1}\in\arg\min_x\varphi_1(x),\quad x_{\varphi_2}\in\arg\min_x\varphi_2(x).
$$

If each φ_i is μ-strongly convex and $\varphi_2-\varphi_1$ is differentiable, then

$$
\frac{\mu}{2}\|x_{\varphi_1}-x_{\varphi_2}\|_2^2\leq\left|(x_{\varphi_1}-x_{\varphi_2})^\top(\nabla(\varphi_2-\varphi_1)(x_{\varphi_1}))\right|.
$$

Proof. For the sake of the proof, we will assume that the FIM and the Hessian are invertible matrices. Under the probabilistic interpretation of the loss elements, the overall loss function for $w^n=\mathbf{1}^{n\setminus i}$ is

$$
L(\mathscr{D},\theta,\lambda,\mathbf{1}^{n\setminus i})\triangleq\frac{1}{n}\sum_{j\neq i}-\log(P\left(y_j|f(x_j;\theta)\right))+\lambda\pi(\theta)
$$

and we assume that $P\left(y|f(x;\theta)\right)$ belongs to an exponential family whose natural parameters are the features $f(x;\theta)$, namely, $\log(P\left(y|f(x;\theta)\right))=f^\top(x;\theta)t(y)-\log(\sum_{\tilde{y}=1}^{|\mathcal{Y}|}\exp\left\{f^\top(x;\theta)t(\tilde{y})\right\})+\beta(y)$ for some natural statistics $t(y)$. For this model, we have

$$
\nabla_\theta\log(P\left(y|f(x;\theta)\right))=\nabla_\theta f(x;\theta)\nabla_f\log(P\left(y|f(x;\theta)\right)).
$$

Thus, the approximated FIM, $\mathbf{F}(\mathscr{D},\theta)$, is given by

$$\begin{aligned}\mathbf{F}(\mathscr{D},\theta) &= \frac{1}{n}\sum_{i=1}^{n}\mathbb{E}_{\mathsf{y}\sim P_{\mathsf{y}|\mathsf{x}=x_i;\theta}}\left[\nabla_\theta f(x_i;\theta)\nabla_f \log(P\left(\mathsf{y}|f(x_i;\theta)\right))\nabla_f^\top \log(P\left(\mathsf{y}|f(x_i;\theta)\right))\nabla_\theta^\top f(x_i;\theta)\right] \\ &= \frac{1}{n}\sum_{i=1}^{n}\nabla_\theta f(x_i;\theta)\mathbb{E}_{\mathsf{y}\sim P_{\mathsf{y}|\mathsf{x}=x_i;\theta}}\left[-\nabla_f^2 \log(P\left(\mathsf{y}|f(x_i;\theta)\right))\right]\nabla_\theta^\top f(x_i;\theta) \qquad \text{(14a)} \\ &= -\frac{1}{n}\sum_{i=1}^{n}\nabla_\theta f(x_i;\theta)\nabla_f^2 \log(P\left(y_i|f(x_i;\theta)\right))\nabla_\theta^\top f(x_i;\theta)\end{aligned}$$

where (14a) is by using classical properties of the exponential family, and where the last equality is since the Hessian of an exponential family with respect to the natural parameters f is independent of y (see App. G). Moreover, we note that the Hessian of the loss is given by

$$\begin{aligned}\mathbf{H}(\theta,\mathbf{1}^{n\setminus i}) &= \nabla_\theta^2 L(\mathscr{D},\theta,\mathbf{1}^{n\setminus i}) \\ &= \nabla_\theta^2 L(\mathscr{D},\theta,\mathbf{1}^{n\setminus i}-\mathbf{1}) + \nabla_\theta^2 L(\mathscr{D},\theta,\mathbf{1}) \\ &= \nabla_\theta^2 L(\mathscr{D},\theta,\mathbf{1}^{n\setminus i}-\mathbf{1}) + \frac{1}{n}\sum_{i=1}^{n}\nabla_\theta^2 f(x_i;\theta)\nabla_f \log(P\left(y_i|f(x_i;\theta)\right)) + \mathbf{F}(\mathscr{D};\theta).\end{aligned}$$

We start by defining the next functions

$$\begin{aligned}\psi_1(\theta) &\triangleq 2L(\mathscr{D},\theta,\lambda,\mathbf{1}^{n\setminus i}) = 2L(\mathscr{D},\theta,\mathbf{1}^{n\setminus i}) + 2\lambda\pi(\theta), \\ \psi_2(\theta) &\triangleq -2b^\top(\hat{\theta}(\mathbf{1}),\mathbf{1}^{n\setminus i})\cdot(\hat{\theta}(\mathbf{1})-\theta) + (\hat{\theta}(\mathbf{1})-\theta)^\top\nabla^2 L(\mathscr{D},\hat{\theta}(\mathbf{1}),\mathbf{1}^{n\setminus i})(\hat{\theta}(\mathbf{1})-\theta) + 2\lambda\pi(\theta), \\ \psi_3(\theta) &\triangleq -2b^\top(\hat{\theta}(\mathbf{1}),\mathbf{1}^{n\setminus i})\cdot(\hat{\theta}(\mathbf{1})-\theta) + (\hat{\theta}(\mathbf{1})-\theta)^\top\cdot\mathbf{F}\cdot(\hat{\theta}(\mathbf{1})-\theta) + 2\lambda\pi(\theta) \\ &= (\theta-(\hat{\theta}(\mathbf{1})-\mathbf{F}^{-1}\cdot b(\hat{\theta}(\mathbf{1}),\mathbf{1}^{n\setminus i})))^\top\mathbf{F}(\theta-(\hat{\theta}(\mathbf{1})-\mathbf{F}^{-1}\cdot b(\hat{\theta}(\mathbf{1}),\mathbf{1}^{n\setminus i}))) + 2\lambda\pi(\theta) + J\end{aligned}$$

where J is a constant (which is independent of θ) and $\mathbf{F}$ is an abbreviation for $\mathbf{F}(\mathscr{D},\hat{\theta}(\mathbf{1}))$. We first note that the minimizer of ψ_1 is $\hat{\theta}(\mathbf{1}^{n\setminus i})$ and that the minimizer of ψ_3 is $\tilde{\theta}(\mathbf{1}^{n\setminus i})$ from (9).

We note that Assump. 1 and Assump. 2 guarantees that the overall loss, L, is μ-strongly convex and that the difference $L(\mathscr{D},\hat{\theta}(\mathbf{1}),\lambda,\mathbf{1}^{n\setminus i}) - L(\mathscr{D},\hat{\theta}(\mathbf{1}),\lambda,\mathbf{1})$ is differentiable. Thus, using Lem. 2, which follows by applying the optimizer comparison lemma with $L(\mathscr{D},\theta,\lambda,\mathbf{1}^{n\setminus i})$ and $L(\mathscr{D},\theta,\lambda,\mathbf{1})$ allows us to derive the following upper bound

$$\|\hat{\theta}(\mathbf{1})-\hat{\theta}(\mathbf{1}^{n\setminus i})\| \leq \frac{2}{n\mu}\cdot\|\nabla_\theta\ell(z_i,\hat{\theta}(\mathbf{1}))\| \triangleq \frac{2g_i}{\mu}. \qquad (15)$$

The optimizer comparison lemma [51, Lem. 1] with ψ_1 and ψ_3 and Cauchy-Schwartz inequality yields

$$\begin{aligned}\frac{\mu}{2}\|\hat{\theta}(\mathbf{1}^{n\setminus i})-\tilde{\theta}(\mathbf{1}^{n\setminus i})\|^2 &\le |(\hat{\theta}(\mathbf{1}^{n\setminus i})-\tilde{\theta}(\mathbf{1}^{n\setminus i}))^\top(\nabla(\psi_3-\psi_1)(\hat{\theta}(\mathbf{1}^{n\setminus i})))| \\ &\le \|\hat{\theta}(\mathbf{1}^{n\setminus i})-\tilde{\theta}(\mathbf{1}^{n\setminus i})\|\|(\nabla(\psi_3-\psi_1)(\hat{\theta}(\mathbf{1}^{n\setminus i})))\|\end{aligned}$$

We divide both sides by $\|\hat{\theta}(\mathbf{1}^{n\setminus i})-\tilde{\theta}(\mathbf{1}^{n\setminus i})\|$, and by using the triangle inequality we get

$$\begin{aligned}&\frac{\mu}{2}\|\hat{\theta}(\mathbf{1}^{n\setminus i})-\tilde{\theta}(\mathbf{1}^{n\setminus i})\| \le \|\nabla(\psi_3-\psi_1)(\hat{\theta}(\mathbf{1}^{n\setminus i}))\| \\ &\quad\le \|\nabla(\psi_3-\psi_2)(\hat{\theta}(\mathbf{1}^{n\setminus i}))+\nabla(\psi_2-\psi_1)(\hat{\theta}(\mathbf{1}^{n\setminus i}))\| && (16)\\ &\quad\le \|\nabla(\psi_3-\psi_2)(\hat{\theta}(\mathbf{1}^{n\setminus i}))\|+\|\nabla(\psi_2-\psi_1)(\hat{\theta}(\mathbf{1}^{n\setminus i}))\| \\ &\quad\le \|\nabla^2 L(\mathscr{D},\hat{\theta}(\mathbf{1}),\mathbf{1}^{n\setminus i})-\mathbf{F}(\mathscr{D},\hat{\theta}(\mathbf{1}))\|\|\hat{\theta}(\mathbf{1})-\hat{\theta}(\mathbf{1}^{n\setminus i})\|+\|(\nabla(\psi_2-\psi_1)(\hat{\theta}(\mathbf{1}^{n\setminus i})))\| \\ &\quad= \|\nabla^2 L(\mathscr{D},\hat{\theta}(\mathbf{1}),\mathbf{1}^{n\setminus i}-\mathbf{1})+\frac{1}{n}\sum_{i=1}^{n}\nabla_\theta^2 f(x_i;\hat{\theta}(\mathbf{1}))\nabla_f\log(P(y_i|f(x_i;\hat{\theta}(\mathbf{1}))))\|\|\hat{\theta}(\mathbf{1})-\hat{\theta}(\mathbf{1}^{n\setminus i})\| \\ &\qquad\qquad+\|(\nabla(\psi_2-\psi_1)(\hat{\theta}(\mathbf{1}^{n\setminus i})))\| \\ &\quad\le \frac{g_i}{n\mu}\cdot\|-\nabla_\theta f(x_i;\hat{\theta}(\mathbf{1}))\nabla_f^2\log(P(y_i|f(x_i;\hat{\theta}(\mathbf{1}))))\nabla_\theta^\top f(x_i;\hat{\theta}(\mathbf{1})) && (17)\\ &\qquad\qquad+\sum_{i=1}^{n}\nabla_\theta^2 f(x_i;\hat{\theta}(\mathbf{1}))\nabla_f\log(P(y_i|f(x_i;\hat{\theta}(\mathbf{1}))))\|+\frac{Mg_i^2}{2\mu^2}\end{aligned}$$

where (16) is since the differences $\psi_3-\psi_2$ and $\psi_2-\psi_1$ are differentiable and where (17) is by using the next bound:

$$\begin{aligned}&\|(\nabla(\psi_2-\psi_1)(\hat{\theta}(\mathbf{1}^{n\setminus i})))\| \\ &= 2\|b(\hat{\theta}(\mathbf{1}),\mathbf{1}^{n\setminus i})+\nabla^2 L(\mathscr{D},\hat{\theta}(\mathbf{1}),\mathbf{1}^{n\setminus i})(\hat{\theta}(\mathbf{1}^{n\setminus i})-\hat{\theta}(\mathbf{1}))-\nabla L(\mathscr{D},\hat{\theta}(\mathbf{1}^{n\setminus i}),\mathbf{1}^{n\setminus i})\| \\ &= 2\|\nabla L(\mathscr{D},\hat{\theta}(\mathbf{1}),\mathbf{1}^{n\setminus i})+\nabla^2 L(\mathscr{D},\hat{\theta}(\mathbf{1}),\mathbf{1}^{n\setminus i})(\hat{\theta}(\mathbf{1}^{n\setminus i})-\hat{\theta}(\mathbf{1}))-\nabla L(\mathscr{D},\hat{\theta}(\mathbf{1}^{n\setminus i}),\mathbf{1}^{n\setminus i})\| && (18a)\\ &\le M\cdot\left\|\hat{\theta}(\mathbf{1}^{n\setminus i})-\hat{\theta}(\mathbf{1})\right\|^2 && (18b)\\ &\le \frac{4Mg_i^2}{\mu^2}\end{aligned}$$

where (18a) is by the structure and the convexity and differentiability assumptions on L, leading to $\nabla L(\mathscr{D},\hat{\theta}(\mathbf{1}),\mathbf{1})=0$, (18b) implied by the Hessian Lipschitzness of L (see also [3, Lem. 1.2.4]) and the last inequality is by Lem. 2.

We further use the triangle inequality to get the next upper bound

$$\begin{aligned}\frac{\mu}{2}\|\hat{\theta}(\mathbf{1}^{n\setminus i})-\tilde{\theta}(\mathbf{1}^{n\setminus i})\| \le \frac{g_i}{n\mu}(&\|\nabla_\theta f(x_i;\hat{\theta}(\mathbf{1}))\nabla_f^2\log(P(y_i|f(x_i;\hat{\theta}(\mathbf{1}))))\nabla_\theta^\top f(x_i;\hat{\theta}(\mathbf{1}))\| \\ &+\sum_{i=1}^{n}\|\nabla_\theta^2 f(x_i;\hat{\theta}(\mathbf{1}))\nabla_f\log(P(y_i|f(x_i;\hat{\theta}(\mathbf{1}))))\|)+\frac{Mg_i^2}{2\mu^2}\end{aligned}$$

and by using Assump. 5, Assump. 7 and the boundedness of the Hessian of the loss relative to the features (see App. B.2) we get the final bound

$$
\begin{aligned}
\|\hat{\theta}(\mathbf{1}^{n\setminus i}) - \tilde{\theta}(\mathbf{1}^{n\setminus i})\| &\leq \frac{2Qg_i}{n\mu^2}\|\nabla_\theta f(x_i;\hat{\theta}(\mathbf{1}))\|^2 + \frac{Mg_i^2}{\mu^3} \\
&\quad + \frac{2g_i}{n\mu^2}\sum_{i=1}^{n}\|\nabla_\theta^2 f(x_i;\hat{\theta}(\mathbf{1}))\nabla_f \log(P(y_i|f(x_i;\hat{\theta}(\mathbf{1}))))\| \\
&\leq \frac{2QC_f^2 g_i}{n\mu^2} + \frac{Mg_i^2}{\mu^3} + \frac{2g_i\tilde{C}_f}{n\mu^2}\sum_{i=1}^{n}\|\nabla_f \log(P(y_i|f(x_i;\hat{\theta}(\mathbf{1}))))\|
\end{aligned}
$$

where Q is a constant s.t. $\left\|\nabla_f^2 \log(P\left(y|f(x;\theta)\right))\right\| \leq Q$. □

We now emphasize how the third term disappears whenever our model interpolates the training data (namely, $\ell(z_i,\hat{\theta}(\mathbf{1})) = 0, \forall i \in [n]$). In that case, we have $P(y_i|f(x_i;\hat{\theta}(\mathbf{1}))) = 1,\ \forall i \in [n]$ [6]. Thus, following the notation of App. G we have that $\mathbb{E}_{\mathsf{y}\sim P_{\mathsf{y}|\mathsf{x}=x_i;\hat{\theta}(\mathbf{1})}}\left[t(\mathsf{y})\right] = t(y_i)$ and since $\nabla_f \log(P(y_i|f(x_i;\hat{\theta}(\mathbf{1})))) = t(y_i) - \mathbb{E}_{\mathsf{y}\sim P_{\mathsf{y}|\mathsf{x}=x_i;\hat{\theta}(\mathbf{1})}}\left[t(\mathsf{y})\right]$ we get that the third term is zero.

F Comment on Lem. 1 When $\pi(\theta)$ is Twice-Differentiable

Whenever $\pi(\theta)$ is twice differentiable, an equivalent argument to that of Lem. 1 can be stated without the usage of a proximal operator. Specifically, since in this case the entire loss elements $\frac{1}{n}\ell(z_i,\theta) + \lambda\pi(\theta)$ can be approximated using a second-order Taylor expansion, and a solution that uses $\mathbf{C}(\hat{\theta}(\mathbf{1}),\mathbf{1}) = \mathbf{F}(\mathscr{D},\hat{\theta}(\mathbf{1})) + \lambda\nabla^2\pi(\hat{\theta}(\mathbf{1}))$ leads to similar arguments as those from App. E. For this approximation we define the solution via

$$
\tilde{\theta}(\mathbf{1}^{n\setminus i}) \triangleq \hat{\theta}(\mathbf{1}) - (\mathbf{F}(\mathscr{D},\hat{\theta}(\mathbf{1})) + \lambda\nabla^2\pi(\hat{\theta}(\mathbf{1})))^{-1} b(\hat{\theta}(\mathbf{1}),\mathbf{1}^{n\setminus i})
$$

and a similar analysis to that of App. E can be carried out and to lead to similar guarantees. An example for such arguments from a similar application can be found in [51, Thm. 2].

G Fisher Information Matrix for Exponential Families

Using the fact that the distribution $P\left(y|f(x;\theta)\right)$ belongs to an exponential family, namely

$$
\log(P\left(y|f(x;\theta)\right)) = f^\top(x;\theta)t(y) - \log\left(\sum_{\tilde{y}=1}^{|\mathcal{Y}|}\exp\left\{f^\top(x;\theta)t(\tilde{y})\right\}\right) + \beta(y),
$$

[6] In the continuous case, this amounts to $P(y_i|f(x_i;\hat{\theta}(\mathbf{1})))$ converging to a delta-function, concentrated around the value y_i

we can directly evaluate the terms $\mathbb{E}_{\mathsf{y}\sim P_{\mathsf{y}|\mathsf{x}=x_i;\theta}}\left[\nabla_f \log(P\left(\mathsf{y}|f(x;\theta)\right))\nabla_f^\top \log(P\left(\mathsf{y}|f(x;\theta)\right))\right]$ and $\mathbb{E}_{\mathsf{y}\sim P_{\mathsf{y}|\mathsf{x}=x_i;\theta}}\left[-\nabla_f^2 \log(P\left(\mathsf{y}|f(x_i;\theta)\right))\right]$ to establish the desired equality. First, we find that:

$$\begin{aligned}\nabla_f \log(P\left(y|f(x;\theta)\right)) &= \nabla_f \left(f^\top(x;\theta)t(y) - \log\left(\sum_{y\in\mathcal{Y}} \exp\left\{f^\top(x;\theta)t(y)\right\}\right)\right)\\ &= t(y) - \mathbb{E}_{\mathsf{y}\sim P_{\mathsf{y}|\mathsf{x}=x_i;\theta}}\left[t(\mathsf{y})\right]\end{aligned}$$

and

$$\begin{aligned}&\mathbb{E}_{\mathsf{y}\sim P_{\mathsf{y}|\mathsf{x}=x_i;\theta}}\left[\nabla_f \log(P\left(\mathsf{y}|f(x;\theta)\right))\nabla_f^\top \log(P\left(\mathsf{y}|f(x;\theta)\right))\right]\\ &\qquad= \mathbb{E}_{\mathsf{y}\sim P_{\mathsf{y}|\mathsf{x}=x_i;\theta}}\left[(t(\mathsf{y}) - \mathbb{E}_{\mathsf{y}\sim P_{\mathsf{y}|\mathsf{x}=x_i;\theta}}\left[t(\mathsf{y})\right])(t(\mathsf{y}) - \mathbb{E}_{\mathsf{y}\sim P_{\mathsf{y}|\mathsf{x}=x_i;\theta}}\left[t(\mathsf{y})\right])^\top\right].\end{aligned}$$

Next, we observe that:

$$\begin{aligned}-\nabla_f^2 \log(P\left(y|f(x;\theta)\right)) &= \nabla_f\left(\frac{\sum_{\tilde{y}\in\mathcal{Y}} t(\tilde{y})\exp\left\{f^\top(x;\theta)t(\tilde{y})\right\}}{\sum_{\tilde{y}_1\in\mathcal{Y}}\exp\left\{f^\top(x;\theta)t(\tilde{y}_1)\right\}}\right)\\ &= \mathbb{E}_{\mathsf{y}\sim P_{\mathsf{y}|\mathsf{x}=x_i;\theta}}\left[t(\mathsf{y})t^\top(\mathsf{y})\right] - (\mathbb{E}_{\mathsf{y}\sim P_{\mathsf{y}|\mathsf{x}=x_i;\theta}}\left[t(\mathsf{y})\right])(\mathbb{E}_{\mathsf{y}\sim P_{\mathsf{y}|\mathsf{x}=x_i;\theta}}\left[t(\mathsf{y})\right])^\top\\ &= \mathbb{E}_{\mathsf{y}\sim P_{\mathsf{y}|\mathsf{x}=x_i;\theta}}\left[(t(\mathsf{y}) - \mathbb{E}_{\mathsf{y}\sim P_{\mathsf{y}|\mathsf{x}=x_i;\theta}}\left[t(\mathsf{y})\right])(t(\mathsf{y}) - \mathbb{E}_{\mathsf{y}\sim P_{\mathsf{y}|\mathsf{x}=x_i;\theta}}\left[t(\mathsf{y})\right])^\top\right].\end{aligned}$$

Moreover, we note that this final result holds for any y. This concludes the proof. □

H Proof of Th. 1

Proof. We start by writing the Taylor expansion of $T(\tilde{\theta}(\mathbf{1}^{n\backslash i}), \mathbf{1}^{n\backslash i})$ around $\hat{\theta}(\mathbf{1}^{n\backslash i})$ to get [7]:

$$\begin{aligned}T(\tilde{\theta}(\mathbf{1}^{n\backslash i}), \mathbf{1}^{n\backslash i}) = T(\hat{\theta}(\mathbf{1}^{n\backslash i}), \mathbf{1}^{n\backslash i}) &+ \nabla_\theta^\top T(\hat{\theta}(\mathbf{1}^{n\backslash i}), \mathbf{1}^{n\backslash i})(\tilde{\theta}(\mathbf{1}^{n\backslash i}) - \hat{\theta}(\mathbf{1}^{n\backslash i})) \qquad (19)\\ &+ \frac{1}{2}(\tilde{\theta}(\mathbf{1}^{n\backslash i}) - \hat{\theta}(\mathbf{1}^{n\backslash i}))^\top \nabla_\theta^2 T(\theta_{\text{mid}}(\mathbf{1}^{n\backslash i}), \mathbf{1}^{n\backslash i})(\tilde{\theta}(\mathbf{1}^{n\backslash i}) - \hat{\theta}(\mathbf{1}^{n\backslash i}))\end{aligned}$$

where $\theta_{\text{mid}}(\mathbf{1}^{n\backslash i}) = \hat{\theta}(\mathbf{1}^{n\backslash i}) + \kappa\cdot(\tilde{\theta}(\mathbf{1}^{n\backslash i}) - \hat{\theta}(\mathbf{1}^{n\backslash i}))$ for some $\kappa \in [0,1]$. By (19) and by the Lipschitz assumptions on T we get

$$\begin{aligned}&\|T(\tilde{\theta}(\mathbf{1}^{n\backslash i}), \mathbf{1}^{n\backslash i}) - T(\hat{\theta}(\mathbf{1}^{n\backslash i}), \mathbf{1}^{n\backslash i})\|\\ &\quad= \|\nabla_\theta^\top T(\hat{\theta}(\mathbf{1}^{n\backslash i}), \mathbf{1}^{n\backslash i})(\tilde{\theta}(\mathbf{1}^{n\backslash i}) - \hat{\theta}(\mathbf{1}^{n\backslash i}))\\ &\qquad\qquad+ \frac{1}{2}(\tilde{\theta}(\mathbf{1}^{n\backslash i}) - \hat{\theta}(\mathbf{1}^{n\backslash i}))^\top \nabla_\theta^2 T(\theta_{\text{mid}}(\mathbf{1}^{n\backslash i}), \mathbf{1}^{n\backslash i})(\tilde{\theta}(\mathbf{1}^{n\backslash i}) - \hat{\theta}(\mathbf{1}^{n\backslash i}))\|\\ &\quad\le \|\nabla_\theta T(\hat{\theta}(\mathbf{1}^{n\backslash i}), \mathbf{1}^{n\backslash i})\|\|\tilde{\theta}(\mathbf{1}^{n\backslash i}) - \hat{\theta}(\mathbf{1}^{n\backslash i})\| \qquad (20a)\\ &\qquad\qquad+ \frac{1}{2}\|\nabla_\theta^2 T(\theta_{\text{mid}}(\mathbf{1}^{n\backslash i}), \mathbf{1}^{n\backslash i})\|_{\text{op}}\|\tilde{\theta}(\mathbf{1}^{n\backslash i}) - \hat{\theta}(\mathbf{1}^{n\backslash i})\|^2\\ &\quad\le C_{T_1}\|\tilde{\theta}(\mathbf{1}^{n\backslash i}) - \hat{\theta}(\mathbf{1}^{n\backslash i})\| + \frac{1}{2}C_{T_2}\|\tilde{\theta}(\mathbf{1}^{n\backslash i}) - \hat{\theta}(\mathbf{1}^{n\backslash i})\|^2. \qquad (20b)\end{aligned}$$

[7] the existence of the Taylor expansion of T is guaranteed by Assump. 6

The proof is completed by substituting (10) into (20b). To prove (12), we write the expansion of $T(\hat{\theta}(\mathbf{1}^{n\setminus i}))$ around $\hat{\theta}(\mathbf{1})$, to get

$$\begin{aligned}
&\|T(\hat{\theta}(\mathbf{1}^{n\setminus i}),\mathbf{1}^{n\setminus i}) - T(\hat{\theta}(\mathbf{1}),\mathbf{1}^{n\setminus i}) - \nabla_\theta T(\hat{\theta}(\mathbf{1}),\mathbf{1}^{n\setminus i})(\tilde{\theta}(\mathbf{1}^{n\setminus i}) - \hat{\theta}(\mathbf{1}))\| \\
&\quad = \|\nabla_\theta T(\hat{\theta}(\mathbf{1}),\mathbf{1}^{n\setminus i})(\tilde{\theta}(\mathbf{1}^{n\setminus i}) - \hat{\theta}(\mathbf{1}^{n\setminus i})) \\
&\qquad\qquad + \frac{1}{2}(\hat{\theta}(\mathbf{1}^{n\setminus i}) - \hat{\theta}(\mathbf{1}))^\top \nabla_\theta^2 T(\tilde{\theta}_{\text{mid}},\mathbf{1}^{n\setminus i})(\hat{\theta}(\mathbf{1}^{n\setminus i}) - \hat{\theta}(\mathbf{1}))\| \\
&\quad \le C_{T_1}\|\tilde{\theta}(\mathbf{1}^{n\setminus i}) - \hat{\theta}(\mathbf{1}^{n\setminus i})\| + \frac{1}{2}C_{T_2}\|\hat{\theta}(\mathbf{1}) - \hat{\theta}(\mathbf{1}^{n\setminus i})\|^2
\end{aligned}$$

where $\tilde{\theta}_{\text{mid}} = \hat{\theta}(\mathbf{1}^{n\setminus i}) + \kappa \cdot (\hat{\theta}(\mathbf{1}) - \hat{\theta}(\mathbf{1}^{n\setminus i}))$ for some $\kappa \in [0,1]$. Substituting (10) and (15) concludes the proof. □

I Proofs of Corol. 1 - Corol. 4

I.1 Proof of Corol. 1

We now show how to use Th. 1 to approximate LOOCV with similar guarantees to the Hessian-based technique from [51]. Throughout the proof, we will use a refined version of (20b), which requires the Lipschitzness of the $T(\cdot,\mathbf{1}^{n\setminus i})$ only at $\hat{\theta}(\mathbf{1})$. We start by defining $\text{ACV} \triangleq \frac{1}{n}\sum_{i=1}^{n}\ell(z_i,\tilde{\theta}(\mathbf{1}^{n\setminus i}))$ and recall that $\text{CV} \triangleq \frac{1}{n}\sum_{i=1}^{n}\ell(z_i,\hat{\theta}(\mathbf{1}^{n\setminus i}))$. Then, similarly to App. H we get

$$\begin{align}
&|\text{ACV} - \text{CV}| \nonumber\\
&= \left|\frac{1}{n}\sum_{i=1}^{n}\ell(z_i,\tilde{\theta}(\mathbf{1}^{n\setminus i})) - \ell(z_i,\hat{\theta}(\mathbf{1}^{n\setminus i}))\right| \nonumber\\
&\le \frac{1}{n}\sum_{i=1}^{n}\left|\ell(z_i,\tilde{\theta}(\mathbf{1}^{n\setminus i})) - \ell(z_i,\hat{\theta}(\mathbf{1}^{n\setminus i}))\right| \nonumber\\
&\le \frac{1}{n}\sum_{i=1}^{n}\left\|\nabla_\theta \ell(z_i,\hat{\theta}(\mathbf{1}^{n\setminus i}))\right\|\left(\frac{2QC_f^2\tilde{g}_i}{n^2\mu^2} + \frac{M\tilde{g}_i^2}{n^2\mu^3} + \frac{2\tilde{g}_i\tilde{C}_f\bar{E}_n}{n\mu^2}\right) \tag{21a}\\
&\qquad\qquad + \frac{1}{2}\text{Lip}(\nabla_\theta \ell(z_i,\theta))\left(\frac{2QC_f^2\tilde{g}_i}{n^2\mu^2} + \frac{M\tilde{g}_i^2}{n^2\mu^3} + \frac{2\tilde{g}_i\tilde{C}_f\bar{E}_n}{n\mu^2}\right)^2 \nonumber\\
&\le \frac{1}{n}\sum_{i=1}^{n}\left(\left\|\nabla_\theta \ell(z_i,\hat{\theta}(\mathbf{1}))\right\| + \text{Lip}(\nabla_\theta \ell(z_i,\theta))\left(\frac{4\tilde{g}_i^2}{n^2\mu^2}\right)\right)\left(\frac{2QC_f^2\tilde{g}_i}{n^2\mu^2} + \frac{M\tilde{g}_i^2}{n^2\mu^3} + \frac{2\tilde{g}_i\tilde{C}_f\bar{E}_n}{n\mu^2}\right) \tag{21b}\\
&\qquad\qquad + \frac{1}{2}\text{Lip}(\nabla_\theta \ell(z_i,\theta))\left(\frac{2QC_f^2\tilde{g}_i}{n^2\mu^2} + \frac{M\tilde{g}_i^2}{n^2\mu^3} + \frac{2\tilde{g}_i\tilde{C}_f\bar{E}_n}{n\mu^2}\right)^2 \nonumber
\end{align}$$

where (21a) is by using (20a) together with the bound from Th. 1 and by replacing the Lipschitz constants C_{T_1} and C_{T_2} of the objective with the corresponding gradients from (20a) and (21b) is by using the Taylor expansion of $\nabla_\theta \ell(z_i, \hat{\theta}(\mathbf{1}^{n\setminus i}))$ around $\hat{\theta}(\mathbf{1})$ and by using Lem. 2. Expanding this expression yields

$$
\begin{aligned}
|\mathrm{ACV} - \mathrm{CV}| \leq{} & \left(\frac{2QC_f^2}{\mu^2 n^2} + \frac{2\tilde{C}_f \bar{E}_n}{\mu^2 n}\right) \cdot \frac{1}{n} \sum_{i=1}^{n} \left\| \nabla_\theta \ell(z_i, \hat{\theta}(\mathbf{1})) \right\|^2 + \left(\frac{M}{\mu^3 n^2}\right) \cdot \frac{1}{n} \sum_{i=1}^{n} \left\| \nabla_\theta \ell(z_i, \hat{\theta}(\mathbf{1})) \right\|^3 \\
& + \left(\frac{8QC_f^2}{\mu^4 n^4} + \frac{8\tilde{C}_f \bar{E}_n}{\mu^4 n^3}\right) \cdot \frac{1}{n} \sum_{i=1}^{n} \mathrm{Lip}(\nabla_\theta \ell(z_i, \theta)) \left\| \nabla_\theta \ell(z_i, \hat{\theta}(\mathbf{1})) \right\|^3 \\
& + \left(\frac{4M}{\mu^5 n^4}\right) \cdot \frac{1}{n} \sum_{i=1}^{n} \mathrm{Lip}(\nabla_\theta \ell(z_i, \theta)) \left\| \nabla_\theta \ell(z_i, \hat{\theta}(\mathbf{1})) \right\|^4 \\
& + \left(\frac{2Q^2C_f^4}{\mu^4 n^4} + \frac{2\tilde{C}_f^2 \bar{E}_n^2}{\mu^4 n^2}\right) \cdot \frac{1}{n} \sum_{i=1}^{n} \mathrm{Lip}(\nabla_\theta \ell(z_i, \theta)) \left\| \nabla_\theta \ell(z_i, \hat{\theta}(\mathbf{1})) \right\|^2 \\
& + \left(\frac{2QC_f^2 M}{n^4 \mu^5}\right) \cdot \frac{1}{n} \sum_{i=1}^{n} \mathrm{Lip}(\nabla_\theta \ell(z_i, \theta)) \left\| \nabla_\theta \ell(z_i, \hat{\theta}(\mathbf{1})) \right\|^3 \\
& + \left(\frac{M^2}{n^4 \mu^6}\right) \cdot \frac{1}{n} \sum_{i=1}^{n} \mathrm{Lip}(\nabla_\theta \ell(z_i, \theta)) \left\| \nabla_\theta \ell(z_i, \hat{\theta}(\mathbf{1})) \right\|^4 \\
& + \left(\frac{M\tilde{C}_f \bar{E}_n}{n^3 \mu^5}\right) \cdot \frac{1}{n} \sum_{i=1}^{n} \mathrm{Lip}(\nabla_\theta \ell(z_i, \theta)) \left\| \nabla_\theta \ell(z_i, \hat{\theta}(\mathbf{1})) \right\|^3 \\
& + \left(\frac{2Q\tilde{C}_f C_f^2 \bar{E}_n}{n^3 \mu^4}\right) \cdot \frac{1}{n} \sum_{i=1}^{n} \mathrm{Lip}(\nabla_\theta \ell(z_i, \theta)) \left\| \nabla_\theta \ell(z_i, \hat{\theta}(\mathbf{1})) \right\|^2
\end{aligned}
$$

whose decay rate is dictated by the first two terms and is given by $O\left(\frac{C_f^2 B_{02}}{\mu^2 n^2} + \frac{\tilde{C}_f \bar{E}_n B_{02}}{\mu^2 n} + \frac{M B_{03}}{\mu^3 n^2}\right)$. □

I.2 Proof of Corol. 2

The proof follows similarly to that from [49] by using the bound $\tilde{g}_i \leq G$ in (10) and then using the Gaussian mechanism for differential privacy [18, App. A]. □

We note that Corol. 2 parallels a similar result to that of Prop. 2, with different Lipschitz constants and with an additional term that depends on $\bar{E}_n$.

I.3 Proof of Corol. 3

The proof is by substituting $\tilde{g}_i = \|\nabla_\theta \ell(z_i, \hat{\theta}(\mathbf{1}))\|$ in (11) and (12) and maximizing over i. □

We note that this proof parallels a similar result to that of Prop. 3, with two additional terms: one that depends on $\bar{E}_n$ and the other that depends on the Lipschitz coefficient of the features C_f.

I.4 Proof of Corol. 4

By using the definition of T from (2) and using the linearity of expectation and the triangle inequality we get that the Lipschitz coefficient of T from (2), C_{T_1}, is given by $2C_f$. Then, the proof follows by substituting $\tilde{g}_i = \|\nabla_\theta \ell(z_i, \hat{\theta}(\mathbf{1}))\|$ in (11) and maximizing over i. □

J The Connection Between Hessian-based IF and AFIF

We now present two results that establish a connection between our AFIF framework and the Hessian-based influence function. First, we will prove that the Hessian-based solution $\tilde{\theta}^{\text{IJ}}(\mathbf{1}^{n\backslash i})$ and our FIM-based solution $\tilde{\theta}^{\text{IJ,AF}}(\mathbf{1}^{n\backslash i})$ are close. Then, we will prove that a similar statement holds with regard to the inference objective, namely, $T(\tilde{\theta}^{\text{IJ}}(\mathbf{1}^{n\backslash i}))$ and $T(\tilde{\theta}^{\text{IJ,AF}}(\mathbf{1}^{n\backslash i}))$ are also closed. These findings suggest that, while our development relies on assumptions that are rarely met in practical applications, the AFIF can effectively replace the Hessian-based IF without altering the conclusions typically drawn from the latter.

J.1 Proof of Closeness of $\tilde{\theta}^{\text{IJ}}(\mathbf{1}^{n\backslash i})$ and $\tilde{\theta}^{\text{IJ,AF}}(\mathbf{1}^{n\backslash i})$

We will prove a slightly modified result that correspond to the definitions from [4]; namely, $\pi(\theta) = \|\theta\|^2$ and where $\tilde{\theta}^{\text{IJ}}(\mathbf{1}^{n\backslash i})$ and $\tilde{\theta}^{\text{IJ,AF}}(\mathbf{1}^{n\backslash i})$ are defined with the regularized matrices and where λ is chosen s.t. $\mathbf{H}(\hat{\theta}(\mathbf{1}), \mathbf{1}) + \lambda\mathbf{I} \succeq 0$ and $\mathbf{F}(\mathscr{D}, \hat{\theta}(\mathbf{1})) + \lambda\mathbf{I} \succeq 0$.

Proof. The proof follows similarly to App. E. We define the functions

$$\psi_1 = -2b^\top(\hat{\theta}(\mathbf{1}), \mathbf{1}^{n\backslash i})(\hat{\theta}(\mathbf{1}^{n\backslash i}) - \theta) + (\hat{\theta}(\mathbf{1}^{n\backslash i}) - \theta)^\top(\mathbf{H}(\hat{\theta}(\mathbf{1}), \mathbf{1}) + \lambda\mathbf{I})(\hat{\theta}(\mathbf{1}^{n\backslash i}) - \theta),$$
$$\psi_2 = -2b^\top(\hat{\theta}(\mathbf{1}), \mathbf{1}^{n\backslash i})(\hat{\theta}(\mathbf{1}^{n\backslash i}) - \theta) + (\hat{\theta}(\mathbf{1}^{n\backslash i}) - \theta)^\top(\mathbf{F}(\mathscr{D}, \hat{\theta}(\mathbf{1})) + \lambda\mathbf{I})(\hat{\theta}(\mathbf{1}^{n\backslash i}) - \theta)$$

whose minimizers correspond to $\tilde{\theta}^{\text{IJ}}(\mathbf{1}^{n\backslash i})$ and $\tilde{\theta}^{\text{IJ,AF}}(\mathbf{1}^{n\backslash i})$ with regularized matrices, respectively. By our PSD assumption, we note that ψ_1 and ψ_2 are strongly convex, and we denote the strong convexity constant by μ. We further assume that Assump. 7 and Assump. 5 hold. Then, using [51, Lem. 1] we get that

$$\begin{aligned}
&\frac{\mu}{2}\|\tilde{\theta}^{\text{IJ}}(\mathbf{1}^{n\backslash i}) - \tilde{\theta}^{\text{IJ,AF}}(\mathbf{1}^{n\backslash i})\|^2 \\
&\quad \le \|\nabla(\psi_2 - \psi_1)(\tilde{\theta}^{\text{IJ,AF}}(\mathbf{1}^{n\backslash i}))\| \\
&\quad \le \|\mathbf{H}(\hat{\theta}(\mathbf{1}), \mathbf{1}) - \mathbf{F}(\mathscr{D}, \hat{\theta}(\mathbf{1}))\| \|\hat{\theta}(\mathbf{1}^{n\backslash i}) - \tilde{\theta}^{\text{IJ,AF}}(\mathbf{1}^{n\backslash i})\| \\
&\quad \le \|\frac{1}{n}\sum_{i=1}^{n} \nabla^2_\theta f(x_i; \hat{\theta}(\mathbf{1})) \nabla_f \log(P(y_i|f(x_i; \hat{\theta}(\mathbf{1}))))\| \|\hat{\theta}(\mathbf{1}^{n\backslash i}) - \tilde{\theta}^{\text{IJ,AF}}(\mathbf{1}^{n\backslash i})\| \\
&\quad \le \frac{\tilde{C}_f}{n}\sum_{i=1}^{n} \|\nabla_f \log(P(y_i|f(x_i; \hat{\theta}(\mathbf{1}))))\| \|\hat{\theta}(\mathbf{1}^{n\backslash i}) - \tilde{\theta}^{\text{IJ,AF}}(\mathbf{1}^{n\backslash i})\| \\
&\quad = \tilde{C}_f \bar{E}_n \|\hat{\theta}(\mathbf{1}^{n\backslash i}) - \tilde{\theta}^{\text{IJ,AF}}(\mathbf{1}^{n\backslash i})\|. \qquad (22)
\end{aligned}$$

The final distance bound can be achieved by substituting (10) into (22). □

We note that this bound tells us that the Hessian-based solution and the FIM-based solution are close up to a term that depends on $\bar{E}_n$ times the distance of the error $\|\hat{\theta}(\mathbf{1}^{n\setminus i}) - \tilde{\theta}^{\mathrm{IJ,AF}}(\mathbf{1}^{n\setminus i})\|$, and gives further insight upon the empirical usage of the FIM in influence assessment tasks as done in [4].

J.2 Proof of Closeness of $T(\tilde{\theta}^{\mathrm{IJ}}(\mathbf{1}^{n\setminus i}), \mathbf{1}^{n\setminus i})$ and $T(\tilde{\theta}^{\mathrm{IJ,AF}}(\mathbf{1}^{n\setminus i}), \mathbf{1}^{n\setminus i})$

We will now proceed to prove a stronger result, claiming that the distance between the inference objective evaluated on $T(\tilde{\theta}^{\mathrm{IJ}}(\mathbf{1}^{n\setminus i}), \mathbf{1}^{n\setminus i})$ and on $T(\tilde{\theta}^{\mathrm{IJ,AF}}(\mathbf{1}^{n\setminus i}), \mathbf{1}^{n\setminus i})$ is small, further justifying the utility of the FIM-based influence measurement.

Proof. The proof follows similarly to the proof of Th. 1. Assume that Assump. 7, Assump. 6 and Assump. 5 hold. Then, similarly to the proof from App. H we use the Taylor expansion of $T(\tilde{\theta}^{\mathrm{IJ}}(\mathbf{1}^{n\setminus i}), \mathbf{1}^{n\setminus i})$ around $\tilde{\theta}^{\mathrm{IJ,AF}}(\mathbf{1}^{n\setminus i})$ to get

$$\begin{aligned}
&\|T(\tilde{\theta}^{\mathrm{IJ}}(\mathbf{1}^{n\setminus i}), \mathbf{1}^{n\setminus i}) - T(\tilde{\theta}^{\mathrm{IJ,AF}}(\mathbf{1}^{n\setminus i}), \mathbf{1}^{n\setminus i})\| \\
&\quad = \|\nabla_\theta^\top T(\tilde{\theta}^{\mathrm{IJ,AF}}(\mathbf{1}^{n\setminus i}), \mathbf{1}^{n\setminus i})(\tilde{\theta}^{\mathrm{IJ,AF}}(\mathbf{1}^{n\setminus i}) - \tilde{\theta}^{\mathrm{IJ}}(\mathbf{1}^{n\setminus i})) \\
&\qquad\qquad + \frac{1}{2}(\tilde{\theta}^{\mathrm{IJ,AF}}(\mathbf{1}^{n\setminus i}) - \tilde{\theta}^{\mathrm{IJ}}(\mathbf{1}^{n\setminus i}))^\top \nabla_\theta^2 T(\theta_{\mathrm{mid}}, \mathbf{1}^{n\setminus i})(\tilde{\theta}^{\mathrm{IJ,AF}}(\mathbf{1}^{n\setminus i}) - \tilde{\theta}^{\mathrm{IJ}}(\mathbf{1}^{n\setminus i}))\| \\
&\quad \le \|\nabla_\theta T(\tilde{\theta}^{\mathrm{IJ,AF}}(\mathbf{1}^{n\setminus i}), \mathbf{1}^{n\setminus i})\|\|\tilde{\theta}^{\mathrm{IJ,AF}}(\mathbf{1}^{n\setminus i}) - \tilde{\theta}^{\mathrm{IJ}}(\mathbf{1}^{n\setminus i})\| \\
&\qquad + \frac{1}{2}\|\nabla_\theta^2 T(\theta_{\mathrm{mid}}, \mathbf{1}^{n\setminus i})\|_{\mathrm{op}}\|\tilde{\theta}^{\mathrm{IJ,AF}}(\mathbf{1}^{n\setminus i}) - \tilde{\theta}^{\mathrm{IJ}}(\mathbf{1}^{n\setminus i})\|^2 \\
&\quad \le C_{T_1}\|\tilde{\theta}^{\mathrm{IJ,AF}}(\mathbf{1}^{n\setminus i}) - \tilde{\theta}^{\mathrm{IJ}}(\mathbf{1}^{n\setminus i})\| + \frac{1}{2}C_{T_2}\|\tilde{\theta}^{\mathrm{IJ,AF}}(\mathbf{1}^{n\setminus i}) - \tilde{\theta}^{\mathrm{IJ}}(\mathbf{1}^{n\setminus i})\|^2 \\
&\quad \le \bar{C}_f \bar{E}_n C_{T_1}\|\hat{\theta}(\mathbf{1}^{n\setminus i}) - \tilde{\theta}^{\mathrm{IJ,AF}}(\mathbf{1}^{n\setminus i})\| + \frac{1}{2}C_{T_2}(\bar{C}_f \bar{E}_n)^2\|\hat{\theta}(\mathbf{1}^{n\setminus i}) - \tilde{\theta}^{\mathrm{IJ,AF}}(\mathbf{1}^{n\setminus i})\|^2
\end{aligned}$$

□

We note that this bound goes to zero whenever the quality of our approximation $\tilde{\theta}^{\mathrm{IJ,AF}}(\mathbf{1}^{n\setminus i})$ improves and whenever $\bar{E}_n \to 0$.

K Experimental Details

All experiments were implemented using the PyTorch [38] framework. The experiments from Sec. 5.1 and Sec. 5.3 ran on NVIDIA A100 GPU, and the experiments from Sec. 5.2 ran on NVIDIA Tesla T4 GPU, demonstrating a consistent improvement in computational time across different GPU platforms. The datasets and models used in our experiments are detailed below.

K.1 Datasets

K.1.1 Adult

We utilized the Adult dataset [17] from

https://archive.ics.uci.edu/ml/machine-learning-databases/adult, to perform the task of predicting whether an individual's income is more than 50,000$ using 14 demographic features such as age, education, marital status, and country of origin. We aimed to keep sex as a sensitive attribute that requires fairness. The dataset contains 48,842 samples, divided into 32561 train samples and 16281 test samples. During pre-processing, we remove the sensitive attribute from the set of input features, discard rows with any missing data, convert textual values to categorical ones, and normalize the numerical data using the `StandardScaler()` function from the `sklearn.preprocessing` module. These pre-processing steps are consistent with those used in previous analyses of this dataset (e.g., [46]). We randomized the sample order by enabling the `Shuffle` option when creating the Dataloaders using `torch.utils.data.DataLoader`, ensuring the data was shuffled before being split into batches. The DP was estimated on the training data.

K.1.2 Insurance

We utilized the insurance dataset [31] from https://www.kaggle.com/datasets/teertha/ushealthinsurancedataset, for predicting the total annual medical expenses of individuals using 5 demographic features from the U.S. Census Bureau. The sensitive attribute is sex. During pre-processing, we remove the sensitive attribute from the set of input features and further standardized the features to be between the range 0 to 1. The data has 1,338 samples with 676 males and 662 females. We use a train-test split ratio 0.8:0.2. We randomized the sample order by enabling the `Shuffle` option when creating the Dataloaders using `torch.utils.data.DataLoader`, ensuring the data was shuffled before being split into batches. The χ^2 was estimated on the training data.

K.1.3 Crime

We utilized the crime dataset [40] from https://archive.ics.uci.edu/dataset/183/communities+and+crime, considers predicting the number of violent crimes per 100K population using socio-economic information of communities in the U.S. The sensitive attribute is the percentage of people belonging to a particular race in the community. During pre-processing, we drop all the samples with the value of sensitive attribute less than 5% to remove any outliers. We also remove the non-predictive attributes and the sensitive attribute from the set of input features, and normalize all attributes to the standardized range of [0, 1]. The resulting data has 1,112 samples, and we use a train-test split ratio 0.8:0.2. We randomized the sample order by enabling the `Shuffle` option when creating the Dataloaders using `torch.utils.data.DataLoader`, ensuring the data was shuffled before being split into batches. The χ^2 was estimated on the training data. s

K.1.4 CIFAR10

We utilized the CIFAR10 [29] dataset as provided by the `torchvision` package in PyTorch. We trained the models without data augmentation. We pre-processed the data using the next three steps: first, we resized the image to have a size of 224 × 224 pixels. Then, we converted the images to tensors using the `transforms.ToTensor()` method. Next, the images were normalized using the `transforms.Normalize()` method. The normalization process adjusts the image data so that the pixel values have a mean of $0.4914, 0.4822$, and 0.4465 and a standard deviation of $0.2023, 0.1994$, and 0.2010 for the red, green, and blue channels, respectively. Lastly, we filtered the dataset by leaving only the images whose label was "plane" or "car". We randomized the sample order by enabling the `Shuffle` option when creating the Dataloaders using `torch.utils.data.DataLoader`, ensuring the data was shuffled before being split into batches.

K.2 Models

All models were trained either using a cross-entropy loss or either using an MSE loss, implemented via `torch.nn.CrossEntropyLoss()` and `torch.nn.MSELoss()`. Moreover, unless specified otherwise, all the experiments were conducted using L_2 regularization, namely, $\pi(\theta) = \|\theta\|^2$, that was incorporated into the loss by the usage of weight-decay and the AdamW optimizer [34].

Two-Layer Classifier: For the tasks described in Sec. 5.1 and Sec. 5.2, we trained a two-layer fully-connected network. For the Adult dataset, we have used a softmax activation, where for the insurance and crime datasets (where the task is regression) we didn't use any activation. The activation function for the hidden layer was chosen as `SeLU` activation. We used two variants of this model:

1. For the task from Sec. 5.1, the width of the hidden layer was chosen to be 1000. We trained the model for 100 epochs using the AdamW optimizer, with a learning rate of 10^{-4}, batches of size 100, momentum parameters $(\beta_1, \beta_2) = (0.9, 0.999)$ and a weight-decay of 10^{-6}.

2. For the task from Sec. 5.2, the width of the hidden layer was chosen to be 30000. We trained the model using the AdamW optimizer, with a learning rate of 10^{-4}, batch size of 100, momentum parameters $(\beta_1, \beta_2) = (0.9, 0.999)$ and a weight-decay of 10^{-8}. We varied the number of epochs from 1 to 10.

CNN: The network comprises two convolutional layers and three fully connected layers, with max pooling operations interleaved between the convolutions. The first convolution layer processes a three-channel input to produce six channels using a 5×5 kernel. This is followed by a max pooling layer with a 2×2 window. The second convolution layer takes the six-channel output and produces sixteen channels using a 5×5 kernel, and is again followed by a 2×2 max pooling layer. After the pooling operations, the output is flattened into a one-dimensional vector. This vector is then passed sequentially through three fully connected layers: the first maps the flattened vector (of size 16×53×53) to 120 units, the second reduces it from 120 to 84 units, and the final layer maps from 84 units to 2 output units. ReLU activation functions are applied after the convolution layers and the first two fully connected layers. The network was trained for 100 epochs on a subset of the CIFAR10 dataset that contains only samples with the label "plane" or "car" using the AdamW optimizer with a learning rate of 10^{-5}, a weight decay of 10^{-6}, and the default momentum parameters $(\beta_1, \beta_2) = (0.9, 0.999)$. The model was trained with a batch size of 128.

ResNet18: We used PyTorch's pre-trained version of ResNet18, initially trained on the

ImageNet dataset, as delivered in the `torchvision.models` library. A fully connected layer of size 1000 × 2 was added, and the whole network (the pre-trained part and the additional output layer) was fine-tuned for 10 epochs on a subset of the CIFAR10 dataset that contains only samples with the label "plane" or "car" using the AdamW optimizer with a learning rate of 10^{-5}, a weight decay of 10^{-6}, and the default momentum parameters $(\beta_1, \beta_2) = (0.9, 0.999)$. The model was trained with a batch size of 128.

K.3 Details for Fairness and Unlearning

We trained the model on the training set of each dataset. Using the trained model, we estimated the fairness metric (either (2) or (3)) on the training data and measured the influence of each sample on this metric using the Taylor series-based approximation. We then selected all indices with a positive influence and unlearned them from the model by applying (9). The vector w^n used for generating $\tilde{\theta}^{\mathrm{IJ,AF}}$ had zeros at the selected indices and ones elsewhere. In all cases, we have measured influence using the `LiSSA` algorithm (see detailed description in [4, 1]), where we have set the depth parameter to 2000 and the number of repetitions to 3. The parameter σ was set to $\frac{1}{500}$ for the Adult dataset, and to $\frac{1}{2000}$ for the Insurance and the Crime datasets. Those parameters were tuned manually for achieving good results for both the Fisher-based and the Hessian-based techniques for each dataset.

K.4 Details for Cross-Validation

We have performed a leave-k-out CV to estimate the test loss. To that end, we first pick a random subset of 6000 training points and generate the leave-k-out estimator by using (9) where $\tilde{\theta}^{\mathrm{IJ,AF}}$ was generated with a vector w^n that contain zeros for the chosen indices and ones everywhere else. Then, we estimated the loss this model has on the samples chosen by using the plug-in estimator and then averaging the loss estimates over the different samples. The final estimate was generated by repeating this process five different times and reporting the averaged estimate across the different experiments.

K.5 Details for Data Attribution

For the data attribution experiments, we used the trained model and calculated the influence scores by using the Taylor series-based approximation for the inference objective $\ell(z_{\text{test}}, \theta) - \ell(z_{\text{test}}, \hat{\theta}(\mathbf{1}))$, namely

$$\mathrm{IF}(z_{\text{test}}, z_i) = -\nabla_\theta^\top \ell(z_{\text{test}}, \hat{\theta}(\mathbf{1}))(\mathbf{C}(\hat{\theta}(\mathbf{1}), \mathbf{1}))^{-1} \nabla_\theta \ell(z_i, \hat{\theta}(\mathbf{1}))$$

where $\mathbf{C}(\hat{\theta}(\mathbf{1}), \mathbf{1})$ is either the Hessian or the approximated FIM.

L Additional Experiments

L.1 Additional Experiments for Sec. 5.1

To further demonstrate the usefulness of our approach, we have repeated the same experiment from Sec. 5.1 but with different scaling factors for the `LiSSA` algorithm. Our goal is to show

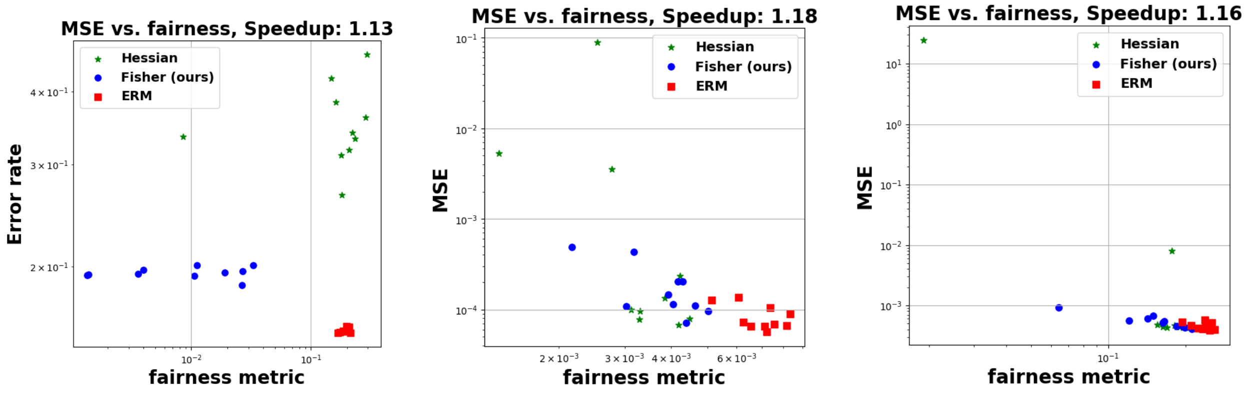

(a) Adult: $\sigma = \frac{1}{200}$ (b) Insurance: $\sigma = \frac{1}{2000}$ (c) Crime: $\sigma = \frac{1}{500}$

Figure 6: Additional experiment results with a reduced value of σ of the LiSSA algorithm. All figures consistently shows the computational advantage of our method and further demonstrate potential instabilities of using the Hessian-based techniques, leading to cases with severely degraded performance.

that in practice the AFIF provides further more stable method for measuring influence. To that end, we have increased the scaling factor of the LiSSA algorithm, which controls its convergence. Following Fig. 6, the Hessian-based method fails to provide a reasonable solution that corrects the model's fairness and provides solutions with inconsistent fairness metrics. On the other hand, our algorithm can reduce fairness while maintaining the model performance and further consistently outperforms the Hessian-based method regarding computational time. This further demonstrates the superiority of our algorithm in terms of computational time and further shows that it requires less hyperparameter tuning.

L.2 Additional Experiments for Sec. 5.2

To demonstrate our claim about the stability of the Hessian-based computations, we have repeated the same experiment from Sec. 5.2 and have decreased the parameter σ of the LiSSA algorithm from $\frac{1}{500}$ to $\frac{1}{750}$. Since this parameter shrinks the inner matrix in the computations, it should help the algorithm to converge in cases where the underlying matrix is poorly conditioned. However, as is demonstrated in Fig. 7, the Hessian-based CV estimator still fails to converge to a reasonable estimate of the test loss. However, we note that under this hyperparameter setting, the Fisher-based algorithm converges to a better estimate of the test loss.

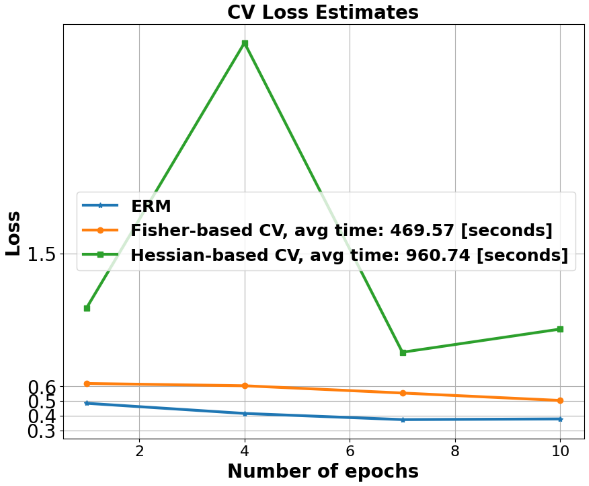

Figure 7: Additional experiment for Sec. 5.2, where the parameter σ of the `LiSSA` was set to $\sigma = \frac{1}{750}$.